The principal CuN_4 "plane" continues to dominate in these five-coordinate ions. The relatively low $A_{\parallel}$ values are consistent with weak *z*-axial interaction through the oxygen donor.

Electrochemical studies are currently in progress. There is evidence for both oxidation to copper(III) and reduction to copper(I). In acetonitrile media for $[Cu(L_2)]^{2+}$, two oxidation features are observed, at 1.34 and 1.745 V, respectively. However, only one reduction peak is seen at −1.1 V. The cyclic voltammograms provide evidence for transient species in intermediate geometry, which may reflect a similar "square" format outlined recently in the electron-transfer reactions of copper(II/I) thioether systems.[34]

Acknowledgment. We thank the NSERC (Canada) and the University of Victoria for financial support.

Supplementary Material Available: Tables S1-S17, containing bond distances and angles, anisotropic temperature parameters, selected intermolecular distances, and experimental crystallographic data for all complexes, and a diagram of the dimeric amidol structure (29 pages); Tables S18-S21, listing calculated and observed structure factors (33 pages). Ordering information is given on any current masthead page.

(34) Bernardo, M. M.; Robandt, P. V.; Schroeder, R. R.; Rorabacher, D. B. *J. Am. Chem. Soc.* **1989**, *111*, 1224.

Contribution from the Department of Chemistry, Massachusetts Institute of Technology, Cambridge, Massachusetts 02139

Effects of a Bridging Dicarboxylate Ligand on the Synthesis and Physical Properties of (μ-Oxo)bis(μ-carboxylato)diiron(III) Complexes†

Robert H. Beer, William B. Tolman, Simon G. Bott, and Stephen J. Lippard*

Received October 25, 1990

The molecule *m*-phenylenedipropionic acid (H_2MPDP), in which two carboxylates are part of the same bridging unit, has been used in the synthesis of diiron(III) oxo protein analogues containing the (μ-oxo)bis(μ-carboxylato)diiron(III) core. The dicarboxylate ligand $MPDP^{2-}$ facilitates the self-assembly synthesis of $[Fe_2O(MPDP)\{HB(pz)_3\}_2]$ and $[Fe_2O(MPDP)B_2Cl_2]$, complexes having terminal bidentate, B, dipyridyl or bis(1-methylimidazol-2-yl)phenylmethoxymethane (BIPhMe, a polyimidazole nitrogen donor), and monodentate chloride ligands. The structural features and physical properties of $[Fe_2O(MPDP)\{HB(pz)_3\}_2]$ and the two $[Fe_2O(MPDP)B_2Cl_2]$ complexes, elucidated in single-crystal X-ray diffraction studies, are very similar to those of the acetate analogue, $[Fe_2O(O_2CCH_3)_2\{HB(pz)_3\}_2]$, indicating that the coordinated $MPDP^{2-}$ ligand preserves the integrity of the (μ-oxo)bis(μ-carboxylato)diiron(III) core. The multidentate ligand does not impart unusual stability to the $[Fe_2O(MPDP)]^{2+}$ core, however, since decomposition to form $[Fe\{HB(pz)_3\}_2]$ occurred during attempts to reduce $[Fe_2O(MPDP)\{HB(pz)_3\}_2]$ electrochemically. Small differences between the spectroscopic properties of $[Fe_2O(MPDP)\{HB(pz)_3\}_2]$ and $[Fe_2O(MPDP)B_2Cl_2]$ complexes can be accounted for by changes in terminal ligation. The coordination of the BIPhMe imidazole nitrogen atoms to the (μ-oxo)bis(μ-carboxylato)diiron(III) center affords a more accurate model of the histidine ligation found in the proteins and more stable complexes than the dipyridyl counterparts. Chloride ion is coordinated cis to the oxo bridge in both $[Fe_2O(MPDP)B_2Cl_2]$ complexes, the position where exogenous ligands and dioxygen bind in the invertebrate respiratory protein hemerythrin (Hr). The presence of this labile ligand facilitates terminal ligand exchange reactions. Crystal data: $[Fe_2O(MPDP)\{HB(pz)_3\}_2]\cdot 5CHCl_3$, triclinic, $P\bar{1}$, a = 12.878 (1) Å, b = 20.301 (1) Å, c = 11.906 (1) Å, α = 96.28 (1)°, β = 106.96 (1)°, γ = 74.33 (1)°, Z = 2; $[Fe_2O(MPDP)(4,4'\text{-}Me_2bpy)_2Cl_2]\cdot 2CH_3CN$, triclinic, $P\bar{1}$, a = 10.941 (1) Å, b = 11.328 (1) Å, c = 18.781 (2) Å, α = 100.34 (1)°, β = 95.66 (1)°, γ = 115.56 (1)°, Z = 2; $[Fe_2O(MPDP)(BIPhMe)_2Cl_2]\cdot 3CHCl_3\cdot CH_3CN$, triclinic, $P\bar{1}$, a = 15.446 (2) Å, b = 16.077 (2) Å, c = 12.453 (2) Å, α = 95.41 (1)°, β = 100.68 (1)°, γ = 93.17 (1)°, Z = 2.

Introduction

Reversible dioxygen binding, formation of a stable tyrosyl radical, and oxidation of methane are among the remarkable variety of functions performed by dinuclear iron oxo centers in the proteins hemerythrin (Hr),[1] ribonucleotide reductase (RR) from *Escherichia coli*,[2] and methane monooxygenase (MMO),[3] respectively. These proteins bind or activate dioxygen at a vacant or labile coordination site in their reduced, $[Fe^{II}Fe^{II}]$ forms. Structural[4] and vibrational spectroscopic[5] studies have established that Hr binds dioxygen as a terminal hydroperoxide ligand coordinated to one iron of the $\{Fe_2O(O_2CR)_2\}^{2+}$ center, with the remaining terminal sites occupied by histidines:

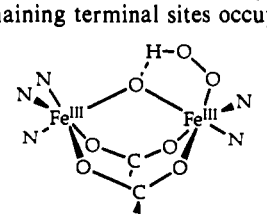

oxyHr

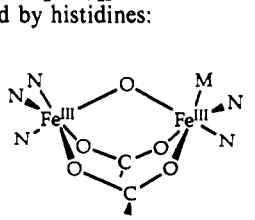

MetMHr

Monodentate (M) anions, including N_3^-, Cl^-, CN^-, OCN^-, and SCN^-, can displace the hydroperoxide ligand, and both the azide adduct and the oxy form of Hr have been crystallographically characterized.[4,6] By analogy to Hr, the diiron centers in RR and MMO probably function by binding and activating dioxygen at a terminal coordination site.

Discovering the principles by which the protein tunes its diiron center either to bind dioxygen reversibly, as in Hr, or to activate dioxygen, as in RR and MMO, is a major objective of current interest in bioinorganic chemistry. One approach to this problem is to prepare and study small molecule analogues containing the dinuclear iron oxo core. Many features of the structural, magnetic,

† Abbreviations used in this article: bpy, 2,2'-dipyridine; 4,4'-Me_2bpy, 4,4'-dimethyl-2,2'-dipyridine; $H_2B(pz)_2^-$, dihydrobis(1-pyrazolyl)borate; TMEDA, *N,N',N'',N'''*-tetramethylethylenediamine; BICOH, bis(1-methylimidazol-2-yl)hydroxymethane; H_2MPDP, *m*-phenylenedipropionic acid; $HB(pz)_3^-$, hydrotris(1-pyrazolyl)borate; BIPhMe, bis(1-methylimidazol-2-yl)phenylmethoxymethane; TMICMe, tris(1-methylimidazol-2-yl)methoxymethane; TICMe, tris(1-imidazol-2-yl)methoxymethane; Me_3TACN, 1,3,7-methyl-1,3,7-triazacyclononane; TIEOH, 1,1,2-tris(1-methylimidazol-2-yl)-ethanol; TMIP, tris(1-methylimidazol-2-yl)phosphine.

(1) (a) Wilkins, P. C.; Wilkins, R. G. *Coord. Chem. Rev.* **1987**, *79*, 195. (b) Klotz, I. M.; Kurtz, D. M., Jr. *Acc. Chem. Res.* **1984**, *17*, 16.
(2) (a) Nordlund, P.; Sjöberg, B.-M.; Ecklund, H. *Nature* **1990**, *345*, 593. (b) Stubbe, J. *J. Biol. Chem.* **1990**, *265*, 5329 and references cited therein. (c) Gräslund, A.; Sahlin, M.; Sjöberg, B.-M. *Environ. Health Perspect.* **1985**, *64*, 139.
(3) (a) Woodland, M. P.; Patil, D. S.; Cammack, R.; Dalton, H. *Biochim. Biophys. Acta* **1986**, *873*, 237. (b) Fox, B. G.; Sererus, K. K.; Münck, E.; Lipscomb, J. D. *J. Biol. Chem.* **1988**, *263*, 10553. (c) Ericson, A.; Hedman, B.; Hodgson, K. O.; Green, J.; Dalton, H.; Bentsen, J. G.; Beer, R. H.; Lippard, S. J. *J. Am. Chem. Soc.* **1988**, *110*, 2330. (d) Prince, R. C.; George, G. N.; Savas, J. C.; Cramer, S. P.; Patel, R. N. *Biochim. Biophys. Acta* **1988**, *952*, 220. (e) Fox, B. G.; Froland, W. A.; Dege, J. E.; Lipscomb, J. D. *J. Biol. Chem.* **1989**, *264*, 10023.
(4) Stenkamp, R. E.; Sieker, L. C.; Jensen, L. H.; McCallum, J. D.; Sanders-Loehr, J. *Proc. Natl. Acad. Sci. U.S.A.* **1985**, *82*, 713.
(5) Shiemke, A. K.; Loehr, T. M.; Sanders-Loehr, J. *J. Am. Chem. Soc.* **1984**, *106*, 4951.
(6) (a) Sheriff, S.; Hendrickson, W. A.; Smith, J. L. *J. Mol. Biol.* **1987**, *197*, 273. (b) Stenkamp, R. E.; Sieker, L. C.; Jensen, L. H. *J. Am. Chem. Soc.* **1984**, *106*, 618.

0020-1669/91/1330-2082$02.50/0

and spectroscopic properties of metN$_3$Hr have been accurately modeled with $\{Fe_2O(O_2CR)_2T_2\}$ complexes (where T is a tridentate ligand).[7] No complete structural and functional synthetic analogue of Hr has been prepared, however, because no existing compound has the two essential requirements for dioxygen binding: the ability to cycle reversibly between $[Fe^{II}Fe^{II}]$ and $[Fe^{III}Fe^{III}]$ oxidation states and a terminal coordination site to bind hydroperoxide.

Early attempts to reproduce the redox behavior found in Hr with $[Fe_2O(O_2CCH_3)_2\{HB(pz)_3\}_2]$ (**1**) failed because of reductive decomposition to a stable mononuclear Fe(II) species, $[Fe\{HB(pz)_3\}_2]$.[8] Only one oxo-bridged complex, $[Fe_2O(O_2CCH_3)_2(Me_3TACN)_2]^{2+}$, is known to undergo reversible redox chemistry.[9] Reductive decomposition is avoided by use of Me_3TACN, which for steric reasons cannot form mononuclear $[Fe(Me_3TACN)_2]^{2+}$. This ligand lacks the terminal imidazole donors in the diiron proteins, however, although it does form a thermodynamically unstable mixed-valent $[Fe^{II}Fe^{III}]$ species. Neither the $HB(pz)_3^-$ nor the Me_3TACN facially coordinating, tridentate terminal ligand affords an open site for dioxygen binding or ligand exchange reactions of the $\{Fe_2O(O_2CR)_2\}^{2+}$ core observed in the diiron proteins. Thus, the development of synthetic routes to diiron(III) compounds, structurally analogous to oxyHr and metMHr, that undergo reversible redox chemistry and allow terminal ligand binding and exchange reactions is an important goal.

Initial efforts to assemble such $[Fe_2O(O_2CR)_2B_2M_2]$ complexes, (R = CH_3, Ph) with terminal bidentate ligands, B, resulted in the isolation of the tetranuclear species $[Fe_4O_2(O_2CR)_7(H_2Bpz_2)_2]^-$,[10] $[Fe_4O_2(O_2CR)_7B_2]^+$ (B = bpy, 4,4′-Me_2bpy, TMEDA),[11,12] and $[Fe_4O_2(O_2CPh)_4(BICO)_2(BICOH)_2]$.[13] The formation of these species was postulated to result from dimerization of two dinuclear intermediates.[10,13] A subsequent communication revealed that $[Fe_4O_2(O_2CCH_3)_7(bpy)_2]^+$ could be cleaved in the presence of excess bpy and chloride, forming $[Fe_2O(O_2CCH_3)_2(bpy)_2Cl_2]$ (**2**).[12] These assembly and cleavage reactions emphasize the facile interconversion of the dinuclear and tetranuclear species.

More recently, we communicated the general synthetic utility of the bridging dicarboxylate ligand *m*-phenylenedipropionic acid (H_2MPDP) for preparing $[Fe_2O(MPDP)T_2]$ and $[Fe_2O(MPDP)B_2M_2]$ complexes under self-assembly conditions.[14] Reported here are full details of our synthetic procedures as well as the results of X-ray crystallographic, magnetic susceptibility, electronic, vibrational, Mössbauer, and NMR spectroscopic, electrochemical, and stability studies of $\{Fe_2O(MPDP)\}^{2+}$ complexes. We discuss how they relate to analogous compounds with monocarboxylate bridging ligands and to Hr. Comparisons are made among different terminal ligand nitrogen and mixed nitrogen/chloride donor sets, and we present the first example of a terminal ligand exchange reaction with the NNM donor set in model complex chemistry.

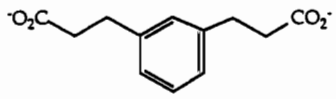

MPDP

Experimental Section

Materials. Bis(1-methylimidazol-2-yl)phenylmethoxymethane (BIPhMe),[15] potassium hydrotris(1-pyrazolyl)borate ($KHB(pz)_3$)[16] and $(Et_4N)_2[Fe_2OCl_6]$[17] were prepared by literature methods. Tris(1-methylimidazol-2-yl)methoxymethane (TMICMe) was obtained by a modification of the reported procedure.[18] Tris(imidazol-2-yl)methoxymethane (TICMe) was prepared by analogy to TMICMe from 1-[(2-(trimethylsilyl)ethoxy)methyl]imidazole.[19] Deuteration of BIPhMe at the *N*-CH_3 and *O*-CH_3 positions to form BIPhMe-d_9 was achieved by using *N*-CD_3Im and CD_3I in the published procedure.[15] *m*-Phenylenedipropionic acid (H_2MPDP) was prepared by hydrogenation of *m*-phenylenediacrylic acid, which was synthesized by a modification[20] of a published procedure.[21] All solvents, reagents, and other chemicals were procured from commercial sources and used without further purification unless otherwise noted. Elemental analyses were performed by Atlantic Microlab, Inc., Atlanta, GA.

Disodium *m*-Phenylenedipropionate (Na_2MPDP). H_2MPDP (16.20 g, 0.073 mmol) was dissolved in 100 mL of EtOH and added with stirring to a solution of NaOEt prepared from Na(s) (3.88 g, 0.169 mol) and 50 mL of EtOH. A white precipitate immediately formed and was stirred for 10 min. The white solid was collected by filtration and washed with EtOH and then with Et_2O to yield 18.48 g of a white powder after drying under vacuum (95%). Anal. Calcd for $C_{12}H_{12}O_4Na_2$: C, 54.14; H, 4.54. Found: C, 53.63; H, 4.90. ^{1}H NMR (CD_3OD, 250 MHz): δ 7.08 (m, 4 H), 2.86 (m, 4 H), 2.43 (m, 4 H). ^{13}C $[^1H]$ NMR (CD_3OD, 68 MHz): δ 181.8, 143.6, 129.3, 129.2, 126.6, 41.0, 33.9. FTIR (KBr): 3017, 2960, 2939, 1556 (s), 1416 (s), 1337, 920, 893, 795, 706, 559, 479 cm^{-1}.

(μ-Oxo)(μ-*m*-phenylenedipropionato)bis(hydrotris(1-pyrazolyl)borato)diiron(III), $[Fe_2O(MPDP)\{HB(pz)_3\}_2]$ (3). Na_2MPDP (0.792 g, 2.98 mmol) was added to a solution of 1.80 g (3.00 mmol) of $(Et_4N)_2[Fe_2OCl_6]$ in 75 mL of CH_3CN and stirred vigorously for 10 min. To the red-brown heterogeneous solution was added 1.512 g (6.00 mmol) of $KHB(pz)_3$ dissolved in 25 mL of CH_3CN dropwise over a 5-min period. The solution darkened and changed to a green-brown color. After the mixture was stirred for 20 min, a red precipitate formed and was removed by filtration. The green-brown filtrate was evaporated and dried under vacuum to yield 2.62 g of a green-brown solid. The solid was stirred with 35 mL of Et_2O and then filtered to give an orange precipitate, which contained a mixture of $[Fe\{HB(pz)_3\}_2]^+$ and the product, as revealed by ^{1}H NMR spectroscopy. The remaining green-brown filtrate was evaporated and dried in vacuo to give 1.258 g of a green-brown solid (54%). To insure that no lattice solvent remained, the product was powdered and dried under vacuum over $CaCl_2$ in a drying pistol with refluxing $CHCl_3$. Anal. Calcd for $C_{30}H_{32}N_{12}B_2O_5Fe_2$: C, 46.56; H, 4.17; N, 21.72. Found: C, 46.34; H, 4.18; N, 21.47. FTIR (KBr): 3142, 3128, 3006, 2970, 2931, 2490, 1556 (s), 1502, 1428 (sh), 1403 (s), 1309, 1214, 1114, 1069, 1049 (s), 980, 756 (s), 716, 663, 621, 522 cm^{-1}. UV/vis [($CHCl_3$) λ, nm (ϵ_{Fe}, cm^{-1} M^{-1})]: 341 (4600), 365 sh, 460 (440), 493 (400), 533 sh, 698 (60).

(μ-Oxo)(μ-*m*-phenylenedipropionato)bis(4,4′-dimethyl-2,2′-dipyridyl)dichlorodiiron(III), $[Fe_2O(MPDP)(4,4'\text{-}Me_2bpy)_2Cl_2]$ (4). A powdered sample of 0.528 g of Na_2MPDP (2.00 mmol) and 1.20 g of $(Et_4N)_2[Fe_2OCl_6]$ (2.00 mmol) was stirred vigorously in 20 mL of CH_3CN forming a red-brown heterogeneous solution. After 5 min, an additional 20 mL of CH_3CN was added. A solution of 0.736 g (4.00 mmol) of 4,4′-Me_2bpy dissolved in 30 mL of CH_2Cl_2 was added to this red-brown mixture dropwise over 5 min. The solution darkened and developed a green color over a 15-min period. After being stirred for 30 min, the solution was filtered and the resulting solid washed with 10 mL of CH_2Cl_2. The combined green filtrates were evaporated under vacuum overnight to obtain 2.195 g of a green solid. This material was dissolved

(7) (a) Lippard, S. J. *Angew. Chem., Int. Ed. Engl.* **1988**, *27*, 344, and references cited therein. (b) Lippard, S. J. *Chem. Br.* **1986**, 222. (c) Sanders-Loehr, J. In *Iron Carriers and Iron Proteins*; Loehr, T. M., Ed.; VCH Publishers: New York, 1989; p 373. (d) Que, L., Jr.; Scarrow, R. C. In *Metal Clusters in Proteins*: Que, L., Jr. Ed.; ACS Symposium Series 372; American Chemical Society: Washington, DC, 1988; p 152. (e) Kurtz, D. M., Jr. *Chem. Rev.* **1990**, *90*, 585. (f) Que, L., Jr.; True, A. E. *Prog. Inorg. Chem.* **1990**, *38*, 97.

(8) Armstrong, W. H.; Spool, A.; Papaefthymiou, G. C.; Frankel, R. B.; Lippard, S. J. *J. Am. Chem. Soc.* **1984**, *106*, 3653.

(9) Hartman, J. R.; Rardin, R. L.; Chaudhuri, P.; Pohl, K.; Wieghardt, K.; Nuber, B.; Weiss, J.; Papaefthymiou, G. C.; Frankel, R. B.; Lippard, S. J. *J. Am. Chem. Soc.* **1987**, *109*, 7387.

(10) Armstrong, W. H.; Roth, M. E.; Lippard, S. J. *J. Am. Chem. Soc.* **1987**, *109*, 6318.

(11) (a) Roth, M. E. Ph.D. Dissertation, Massachusetts Institute of Technology, 1988. (b) Micklitz, W.; Lippard, S. J. Unpublished results.

(12) Vincent, J. B.; Huffman, J. C.; Christou, G.; Li, Q.; Nanny, M. A.; Hendrickson, D. N.; Fong, R. H.; Fish, R. H. *J. Am. Chem. Soc.* **1988**, *110*, 6898.

(13) Gorun, S. M.; Lippard, S. J. *Inorg. Chem.* **1988**, *27*, 149.

(14) (a) Beer, R. H.; Tolman, W. B.; Bott, S. G.; Lippard, S. J. *Inorg. Chem.* **1989**, *28*, 4557. (b) Beer, R. H. Ph.D. Dissertation, Massachusetts Institute of Technology, 1990.

(15) (a) Tolman, W. B.; Bino, A.; Lippard, S. J. *J. Am. Chem. Soc.* **1989**, *111*, 8522. (b) Tolman, W. B.; Liu, S.; Bentsen, J. G.; Lippard, S. J. *J. Am. Chem. Soc.* **1991**, *113*, 152.

(16) Trofimenko, S. *Inorg. Synth.* **1970**, *12*, 99.

(17) Armstrong, W. H.; Lippard, S. J. *Inorg. Chem.* **1985**, *24*, 981.

(18) Sorrell, T. N.; Borovik, A. S. *J. Am. Chem. Soc.* **1987**, *109*, 4255.

(19) (a) Lipshutz, B. M.; Vaccaro, W.; Huff, B. *Tetrahedron Lett.* **1986**, *27*, 4095. (b) Whitten, J. P.; Matthews, D. P.; McCarthy, J. R. *J. Org. Chem.* **1986**, *51*, 1891.

(20) Gensler, W. J.; Berman, E. *J. Am. Chem. Soc.* **1958**, *80*, 4949.

(21) Schimelpfenig, C. W. *J. Org. Chem.* **1975**, *40*, 1493 and references therein.

Table I. Crystallographic Information for $[Fe_2O(MPDP)(HBpz_3)_2]\cdot 5CHCl_3$ (**3**·5CHCl$_3$), $[Fe_2O(MPDP)(4,4'\text{-}Me_2bpy)_2Cl_2]\cdot 2CH_3CN$ (**4**·2CH$_3$CN), and $[Fe_2O(MPDP)(BIPhMe)_2Cl_2]\cdot 3CHCl_3\cdot CH_3CN$ (**5**·3CHCl$_3$·CH$_3$CN)[a]

	3·5CHCl$_3$	**4**·2CH$_3$CN	**5**·3CHCl$_3$·CH$_3$CN
formula	$C_{35}H_{36}B_2N_{12}O_5Cl_{15}Fe_2$	$C_{40}H_{42}N_6O_5Cl_2Fe_2$	$C_{49}H_{54}N_9O_7Cl_{11}Fe_2$
fw	1370.9	869.41	1382.70
space group[b]	$P\bar{1}$ (No. 2)	$P\bar{1}$ (No. 2)	$P\bar{1}$ (No. 2)
a, Å	12.878 (1)	10.941 (1)	15.446 (2)
b, Å	20.301 (1)	11.328 (1)	16.077 (2)
c, Å	11.906 (1)	18.781 (2)	12.453 (2)
α, deg	96.28 (1)	100.34 (1)	95.41 (1)
β, deg	106.96 (1)	95.66 (1)	100.68 (1)
γ, deg	74.33 (1)	115.56 (1)	93.17 (1)
V, Å^3	2865 (1)	2025 (1)	3017 (1)
Z	2	2	2
D_{calcd} (D_{measd}), g cm^{-1}	1.589 (*c*)	1.426 (1.43 (1))	1.522 (1.52 (1))
abs coeff, cm^{-1}	11.74	8.97	10.26
data collcd	$3 < 2\theta < 47°$ $+h,\pm k,\pm l$	$2 < 2\theta < 50°$ $+h,\pm k,\pm l$	$3 < 2\theta < 50°$ $+h,\pm k,\pm l$
no. of data collcd	9378	7490	11161
R_{av}	0.052	0.031	0.064
no. of unique data	8465	7080	10601
no. of unique data with $I > 3\sigma(I)$	4823	4153	5307
no. of var param	682	496	703
R_1[d]	0.060	0.047	0.053
R_2	0.066	0.048	0.065

[a] All measurements were made at room temperature, except for **5**·3CHCl$_3$·CH$_3$CN (−79 °C), by using an Enraf Nonius CAD-4F κ-geometry diffractometer and Mo Kα (0.71073 Å) radiation. [b] Hahn, T., Ed. *International Tables for X-ray Crystallography*, D. Reidel: Dordrecht, The Netherlands 1983. [c] Not determined. [d] $R_1 = \sum||F_o| - |F_c||/\sum|F_o|$; $R_2 = [\sum w||F_o| - |F_c||^2/\sum w|F_o|^2]^{1/2}$, where $w = 4F^2/\sigma^2(F^2)$ and $\sigma(F^2) = (Lp)^{-1}(C + {}^1/_4(t_c/t_b)^2(b_1 + b_2) + (pI)^2)^{1/2}$, where C = total number of counts, t_c = time spent counting peak intensity, t_b = time spent counting one side of background, b_1 = high-angle background counts, b_2 = low-angle background counts, p = fudge factor (fixed at 0.05 except for **4**·2CH$_3$CN where the value was 0.03), and $I = C - {}^1/_2(t_c/t_b)(b_1 + b_2)$.

in 15 mL of CH_2Cl_2, and then 150 mL of CH_3CN was added with swirling. The solution was allowed to stand at room temperature, yielding green crystals, which were filtered and washed with a minimum amount of CH_3CN, followed by Et_2O. Evaporation of the filtrate and crystallization from CH_2Cl_2/CH_3CN as above yielded a total of 0.847 g of product after powdering and drying in vacuo (54%). Anal. Calcd for $C_{36}H_{36}N_4O_5Cl_2Fe_2$: C, 54.92; H, 4.61; N, 7.12; Cl, 9.01. Found: C, 54.64; H, 4.69; N, 7.13; Cl, 8.95. FTIR (KBr): 3053, 3030, 2960, 2926, 1617 (s), 1570 (s), 1560 (s), 1488, 1443 (sh), 1416 (s), 1306, 1289, 1243, 1023, 922, 833, 753, 554, 519 cm^{-1}. UV/vis [(CH_2Cl_2) λ, nm (ϵ_{Fe}, cm^{-1} M^{-1})]: 328 sh, 365 sh, 462 (450), 483 (400), 535 sh, 655 (70), 950 (4.3).

(μ-Oxo)(μ-*m*-phenylenedipropionato)bis(bis(1-methylimidazol-2-yl)-phenylmethoxymethane)dichlorodiiron(III), $[Fe_2O(MPDP)(BIPhMe)_2Cl_2]\cdot H_2O$ (5·H$_2$O). A solution of 0.060 g of powdered $(Et_4N)_2[Fe_2OCl_6]$ (0.10 mmol) and 0.026 g of Na_2MPDP (0.10 mmol) were stirred in 1.5 mL of CH_3CN for 10 min to yield a red-brown heterogeneous mixture. A 1.5-mL solution of 0.056 g of BIPhMe (0.20 mmol) in CH_2Cl_2 was added to this mixture and the color gradually changed from red-brown to green over 30 min. After 20 min of stirring, the green solution was filtered and allowed to stand; attempts to evaporate the solvent and work up the resulting green solid resulted in decomposition to an insoluble green precipitate. After 1 day, microcrystals appeared, which were collected by filtration and washed with 3 × 2 mL portions of CH_3CN. The green microcrystals were powdered and dried under vacuum at 65–70 °C for 1 day to yield 0.050 g of a green powder (50%). Anal. Calcd for $C_{44}H_{50}N_8O_8Cl_2Fe_2$: C, 52.77; H, 5.03; N, 11.19; Cl, 7.08. Found: C, 52.91; H, 4.86; N, 11.27; Cl, 7.15. FTIR (KBr): 3117, 2960 (br), 1630 (br, w), 1573, 1500, 1447, 1407, 1282, 1069, 989, 899, 763, 722, 704 cm^{-1}; difference FTIR (Nujol mull): 3420 (OH) cm^{-1}. UV/vis [($CHCl_3$) λ, nm (ϵ_{Fe}, cm^{-1} M^{-1})]: 341 (3000), 360 sh, 483 (400), 525 sh, 682 (90).

(μ-Oxo)(μ-*m*-phenylenedipropionato)bis(tris(1-methylimidazol-2-yl)-methoxymethane)dichlorodiiron(III), $[Fe_2O(MPDP)(TMICMe)_2Cl_2]\cdot H_2O$ (6·H$_2$O). A 0.150-g (0.25-mmol) portion of powdered $(Et_4N)_2[Fe_2OCl_6]$ and 0.066 g of Na_2MPDP (0.025 mmol) were combined and stirred in 4 mL of CH_3CN for approximately 10 min, forming a red-brown heterogeneous solution. To this mixture, a 4 mL solution of 0.143 g of TMICMe (0.050 mmol) was added. The color of the solution gradually changed from red-brown to green and a white precipitate deposited. After 20 min of stirring, the solution was evaporated under vacuum. The resulting green solid was dissolved in 2 mL of CH_2Cl_2, filtered, and allowed to stand in a capped glass vial overnight as the product precipitated. A green powder was collected by filtration and washed with 10 mL of CH_3CN and dried under vacuum; yield, 0.151 g (60%). Anal. Calcd for $C_{40}H_{50}N_{12}O_8Cl_2Fe_2$: C, 47.59; H, 4.99; N, 16.65; Cl, 7.02. Found: C, 47.52; H, 5.21; N, 16.59; Cl, 7.07. FTIR (KBr): 3116, 2940 (br), 1624 (w, br), 1570, 1499, 1432 (sh), 1410, 1281, 1144 (w), 1075, 991, 902, 756 (br) cm^{-1}; difference FTIR (Nujol mull): 3428 (OH) cm^{-1}. UV/vis [($CHCl_3$) λ, nm (ϵ_{Fe}, cm^{-1} M^{-1})]: 335 (3220), 356 sh, 475 (380), 485 (350), 684 (60).

***cis*-Dichlorobis(tris(imidazol-2-yl)methoxymethane)iron(III) Chloride, $[Fe(TICMe)_2Cl_2]Cl$ (7).** A mixture of TICMe (36 mg, 0.147 mmol) and $FeCl_3\cdot 6H_2O$ (20 mg, 0.074 mmol) was dissolved in MeOH (1 mL) to afford an orange solution. Vapor diffusion of Et_2O into the MeOH solution gave orange prisms of product (30 mg, 62% yield). FTIR (KBr) 2600–3200 (br), 1553, 1464, 1375, 1279, 1264, 1111, 1060, 1026, 991, 952, 897, 772, 754, 739, 712, 691 cm^{-1} UV/vis [(MeOH) λ_{max}, nm (ϵ_{Fe}, cm^{-1} M^{-1})]: 332 (sh), 358 (3200) nm. Anal. Calcd for $C_{22}H_{24}Cl_3FeN_{12}O_2$: C, 40.61; H, 3.72; N, 25.38; Cl, 16.34. Found: C, 40.67; H, 3.88; N, 25.71; Cl, 16.27.

Terminal Ligand Exchange Reactions. Preparation of 3 from 4. A 0.085-g (0.34-mmol) portion of solid $KHB(pz)_3$ was added to a stirring 5-mL solution of 0.125 g of **4** (0.16 mmol) in CH_2Cl_2. The solution immediately turned from green to green-brown and a white precipitate formed. After being stirred for an additional 30 min, the solution was filtered, and the filtrate was evaporated to give a green-brown solid. Et_2O was added in portions (20 mL total) and the solution filtered leaving behind a small amount of red-brown precipitate. The green-brown filtrate was evaporated and dried under vacuum to give a green-brown solid. The solid was stirred with 5 mL of Et_2O for 15 min and then filtered and dried under vacuum to afford 0.108 g of **3** (88%). Anal. Calcd for $C_{30}H_{32}N_{12}B_2O_5Fe_2$: C, 46.56; H, 4.17; N, 21.72. Found: C, 46.21; H, 4.21; N, 21.36.

Crystallographic Studies. Data collection and reduction for compounds **3**-**5**, including corrections of Lorentz and polarization effects, were performed by using general procedures previously described.[22] Relevant crystallographic information is summarized in Table I. Final positional and thermal parameters are supplied in Tables S1–S6 (supplementary material). An abbreviated list of bond distances and angles is given in Tables II and III. A full list of bond distances and angles, as well as calculated and observed structure factor amplitudes for all compounds may be found in Tables S7–S12 (supplementary material). Compounds **4** and **5** were refined by using the TEXSAN software package.[23] Programs provided by SHELX-76 were used to refine **3**.[24] The

(22) Silverman, L. D.; Dewan, J. C.; Giandomenico, C. M.; Lippard, S. J. *Inorg. Chem.* **1980**, *19*, 3379.
(23) TEXRAY Structure Analysis Package, Molecular Structure Corp., College Station, TX, 1985.
(24) Sheldrick, G. M. SHELX-76. In *Computing In Crystallography*; Schenck, H., Olthof-Hazekamp, R., van Konigsveld, H., Bassi, G. C., Eds.; Delft University Press: Delft, The Netherlands, 1978; p 34.

Table II. Selected Interatomic Distances (Å) and Angle (deg) for Compounds **1**–**5** and metN$_3$myoHr[a]

	1	2[b]	3	4	5	metN$_3$myoHr[c]
Fe–O	1.780 (2)	1.783 (4)	1.797 (4)	1.771 (3)	1.783 (5)	1.77
	1.788 (2)	1.787 (4)	1.793 (5)	1.774 (3)	1.790 (4)	1.80
Fe–Cl		2.389 (2)		2.358 (2)	2.428 (2)	
		2.360 (2)		2.376 (2)	2.413 (2)	
Fe–O–Fe	123.6 (1)	123.9 (2)	123.4 (3)	124.0 (2)	125.9 (2)	130
Fe···Fe	3.146 (1)	3.151 (1)	3.161 (1)	3.130 (1)	3.183 (2)	3.23
Fe–N_{cis}(av)	2.153 (3)	2.151 (5)	2.135 (7)	2.155 (4)	2.119 (5)	2.13
Fe–N_{trans}(av)	2.188 (3)	2.208 (5)	2.211 (7)	2.200 (4)	2.159 (6)	2.24
Fe–$O_{CO_2^-}$(av)	2.043 (4)	2.045 (4)	2.053 (5)	2.100 (4)	2.077 (5)	2.10
Fe–$O_{CO_2^-trans}$(av)		2.080 (4)		2.177 (4)	2.109 (5)	2.18
Fe–$O_{CO_2^-cis}$(av)		2.010 (4)		2.025 (3)	2.045 (5)	2.05

[a] Chart I designates the atom labels in Table II. Numbers in parentheses are estimated standard deviations in the last significant digit(s). [b] Reference 12. [c] Reference 6.

Table III. Selected Interatomic Bond Angles (deg) for Compounds **1** and **3**–**5**[a]

	1	3	4	5
N_{trans}–Fe–O	177.4 (1)	175.7 (3)	165.4 (2)	174.4 (2)
N_{cis}–Fe–$O_{CO_2^-trans}$	166.8 (1)	166.7 (2)	168.8 (1)	168.8 (2)
N_{cis}–Fe–$O_{CO_2^-cis}$			163.6 (1)	168.3 (2)
N_{cis}–Fe–N_{trans}	82.2 (1)	81.8 (2)	74.0 (2)	82.4 (2)
$O_{CO_2^-trans}$–Fe–$O_{CO_2^-cis}$	91.0 (1)	91.0 (2)	84.0 (1)	87.6 (2)
O–Fe–N_{cis}	95.9 (1)	96.0 (2)	91.7 (2)	92.7 (2)
O–Fe–X			97.9 (2)	96.6 (2)
O–Fe–$O_{CO_2^-trans}$	96.8 (1)	96.8 (2)	93.1 (2)	94.7 (2)
O–Fe–$O_{CO_2^-cis}$			102.9 (1)	97.3 (2)
X–Fe–N_{cis}	84.4 (1)	85.7 (3)	85.7 (3)	94.7 (1)
X–Fe–N_{trans}	82.2 (1)	81.8 (2)	86.5 (2)	93.1 (1)

[a] Chart I designates the atom labels in Table II. All angles that are not unique were averaged. Numbers in parentheses are estimated standard deviations in the last significant digit(s).

positions of all non-hydrogen atoms were refined with anisotropic thermal parameters unless otherwise specified. All hydrogen atom positions were generated from the coordinates of the carbon atoms to which they were attached with d(C–H) = 0.95 Å unless otherwise specified. When possible, a hydrogen atom for a methyl group was found in the difference map to fix the methyl group hydrogen atom geometry.

$[Fe_2O(MPDP)\{HB(pz)_3\}_2]\cdot 5CHCl_3$ ($3\cdot 5CHCl_3$). X-ray quality, rectangular green crystals of **3** were grown by cooling concentrated solutions of $CHCl_3$ at −20 °C. A crystal of dimensions 0.10 × 0.25 × 0.30 mm was sealed in a glass capillary to prevent solvent loss. An empirical absorption correction was applied to the data. The structure was solved with the direct-methods program MULTAN. All non-hydrogen atoms were located from difference Fourier maps prior to refinement. The hydrogen atoms attached to the boron atoms were found in the difference map and refined isotropically. Two solvent molecules were disordered, resulting in large thermal parameters for several chlorine atoms. One $CHCl_3$ (C2) was refined in a 20:80 ratio; the other molecule, $CHCl_3$ (C5), was not since the atoms of the minor constituent of the disordered chlorine atoms had less than 1 e/Å^3. The largest ratio of parameter shift to esd in the final refinement cycle was 0.505 for a disordered chlorine atom. The final difference map showed no residual electron density greater than 0.67 e/Å^3.

$[Fe_2O(MPDP)(4,4'\text{-}Me_2bpy)_2Cl_2]\cdot 2CH_3CN$ ($4\cdot 2CH_3CN$). X-ray quality green crystals of **4** were grown from solutions of CH_2Cl_2/CH_3CN at room temperature. An irregular polygon with dimensions 0.17 × 0.3 × 0.5 mm was mounted in a glass capillary with a drop of CH_3CN. An empirical absorption correction was applied to the data. The structure was solved by using the direct-methods program MITHRIL. The final difference map showed no residual electron density greater than 0.42 e/Å^3 near Fe2.

$[Fe_2O(MPDP)(BIPhMe)_2Cl_2]\cdot 3CHCl_3\cdot CH_3CN$ ($5\cdot 3CHCl_3\cdot CH_3CN$). X-ray quality green parallelepiped crystals of **5** were grown from solutions of $CHCl_3/CH_3CN$. A crystal with dimensions of 0.16 × 0.35 × 0.05 mm was fixed to the end of a glass fiber with grease under a cold stream of nitrogen. An analytical absorption correction was applied to the data. The structure was solved by using the direct-methods program in SHELXS-86. The final difference map showed no residual electron density greater than 0.48 e/Å^3 near a methoxide group.

Physical Measurements. Cyclic voltammetry experiments were performed with a Princeton Applied Research Model 173 potentiostat and Model 175 universal programmer, and recorded on a Houston Instruments Model 2000 X-Y recorder. The 1–4 mM solutions of compounds used were prepared in methylene chloride (Burdick and Jackson) with 0.2 M tetra-*n*-butylammonium perchlorate (TBAP) or 0.2 M tetra-*n*-butylammonium hexafluorophosphate (TBAH) as supporting electrolyte. A three-electrode configuration was used, comprised of a platinum-disk or glassy-carbon working electrode, a platinum-wire auxiliary electrode, and a Ag/AgCl reference electrode fitted with a Vycor plug at the solution junction. Electrode performance was monitored by observing the ferrocene (Fc^+/Fc) couple. Experiments were carried out at room temperature (~22 °C) under dinitrogen. Rinsing the electrode with solvent and wiping with a tissue after each single scan were sufficient to remove any film that may have deposited on the electrodes as a result of compound decomposition.

A Spex 1401 double monochromator equipped with a cooled RCA 31034 photomultiplier tube with photon-counting electronics was used in the collection of Raman spectra. The spectrometer and the data were manipulated by a locally written program[25] on a Digital Micro PDP 11/73 computer. Tunable argon and krypton lasers, Innovia Models 70 and 90, respectively, were used to obtain Raman spectra of solutions in a spinning 5-mm NMR tube by using a back-scattering geometry. Solutions of **4** underwent photodecomposition, forming precipitates that made it difficult to obtain good quality spectra. This effect was more pronounced at higher energy excitation wavelengths and concentrations. The power incident upon the sample was varied from 20–100 mW, and the monochromator slits were set at 250/300/250 μm. Carbon–chlorine stretching frequencies of methylene chloride and chloroform solvents were used as reference.

^{1}H NMR spectra were recorded at room temperature (~298 K) on Bruker WM250 and Varian XL300 spectrometers. Delay times could be reduced to 0.5 s or less because of the fast relaxation properties of the paramagnetic complexes, shortening the length of time required to collect data. The spin–lattice relaxation rates (T_1) of ^{1}H NMR resonances were determined by the conventional inversion recovery (180°–τ–90°) pulse sequence on a Varian XL 300 instrument.

Ultraviolet and visible spectra were obtained on a Varian Lamba 7 instrument, and near-infrared spectra were recorded with a Perkin-Elmer Model 300 spectrometer. Fourier transform infrared spectra of KBr pellets were recorded and manipulated on a Mattson Cygnus 400 instrument.

Mössbauer spectra were measured at the Francis Bitter National Magnet Laboratory in a BN matrix at 80 and 4.2 K with a conventional constant-acceleration spectrometer equipped with a temperature controller maintaining temperatures within 0.1 K and a γ-ray source of ^{57}Co in Rh.

Solid-state measurements of powdered samples were made at the Francis Bitter National Magnet Laboratory with an SHE Model 905 SQUID susceptometer operating from 1 to 50 kG. A total of 40–50 data points were taken over a 5–300 K temperature range. The moment of the sample holder, an Al–Si bucket, was measured under the same conditions and subtracted from that of the sample. Diamagnetic corrections of 314 × 10^{-6} (**3**), 406 × 10^{-6} (**4**), 625 × 10^{-6} (**5**), and 314 × 10^{-6} (**6**) cgsu mol^{-1} were calculated from Pascal's constants.[26] The data were fit to the theoretical expressions (vide infra) with a nonlinear least-squares method by using a locally written program.[27]

Results and Discussion

Ligand Design and Complex Syntheses. The design of a ligand having the two bridging acetate groups of the $\{Fe_2O(O_2CCH_3)_2\}^{2+}$ moiety as part of the same molecule was based upon a combination

(25) Program RM2, George R. Harrison Spectroscopy Laboratory at MIT.
(26) (a) Carlin, R. L. In *Magnetochemistry*; Springer-Verlag: New York, 1986; p 3. (b) O'Connor, C. J. *Prog. Inorg. Chem.* **1982**, *29*, 203.
(27) Karlin, K. Ph.D. Dissertation, Columbia University, 1975.

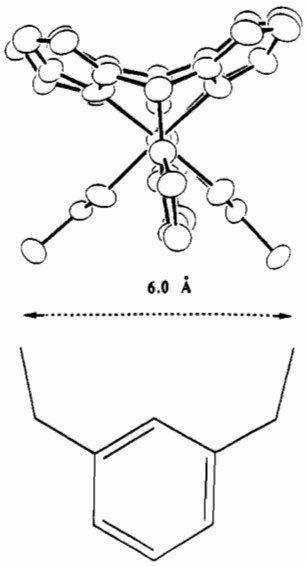

Figure 1. View down the Fe···Fe axis of $[Fe_2O(O_2CCH_3)_2\{HB(pz)_3\}_2]$ (**1**) used in the design of the *m*-phenylene moiety to span the 6.0-Å distance of the two methyl groups of the acetate ligands.

of model building and an analysis of the X-ray structure of **1**.[8] The strategy was to devise the linking portion with proper dimensions to span the distance between the two methyl carbon atoms of the bridging acetate groups in **1**. These methyl groups are separated by a rather long distance of 6.0 Å and are directed away from one another, as illustrated by a view of **1** down the Fe···Fe axis (Figure 1). A rigid *m*-xylyl group provides the appropriate spacer between the α-methylene carbon atoms of each carboxylate functionality.

The dicarboxylic acid *m*-phenylenedipropionic acid (H_2MPDP) is a known compound,[21] but had apparently not been previously used as a ligand. Although chosen to allow binding of its carboxylates to the $\{Fe_2O\}^{4+}$ core (vide supra), $MPDP^{2-}$ is not preorganized to adopt such a conformation prior to coordination. Because of this flexibility and the variety of known binding modes[28] for carboxylates, we recognized the possibility of forming unwanted polynuclear complexes from undesired conformations of the $MPDP^{2-}$ ligand. In related work, several attempts to employ a hexadentate ligand, HL, having two tridentate, facially coordinating ligands connected by a flexible linker afforded a dimer of dinuclear centers, $[\{Fe_2O(O_2CCH_3)_2\}_2(HL)_2]^{4+}$, rather than the desired $[Fe_2O(O_2CR)_2(HL)]^{2+}$ complex.[29]

Despite this caveat, the synthesis of **3** from Na_2MPDP and $(Et_4N)_2[Fe_2OCl_6]$ proceeded as planned (eq 1). The reaction

$$(Et_4N)_2[Fe_2OCl_6] + Na_2(MPDP) + 2KHB(pz)_3 \rightarrow [Fe_2O(MPDP)\{HB(pz)_3\}_2] + 2Et_4NCl + 2KCl + 2NaCl \quad (1)$$

was carried out under self-assembly conditions in which equal amounts of the dicarboxylate ligand and the (μ-oxo)diiron(III) starting material were combined in acetonitrile to form a red-brown heterogeneous mixture prior to the addition of 2 equiv of $KHB(pz)_3$. The major product is **3**, which can be isolated by extracting the crude material with diethyl ether, leaving the undesired $[Fe\{HB(pz)_3\}_2]^+$ product behind. The same reaction carried out in water with $Fe(ClO_4)_3 \cdot 10H_2O$ used as the iron source, analogous to the method first employed to prepare $[Fe_2O(O_2CCH_3)_2\{HB(pz)_3\}_2]$,[8] produced primarily $[Fe\{HB(pz)_3\}_2]^+$.

The syntheses of $[Fe_2O(MPDP)B_2Cl_2]$ complexes were carried out under the same self-assembly conditions used to prepare **3** but with a bidentate nitrogen donor B = 4,4′-Me_2bpy, BIPhMe, or TMICMe substituted in place of $HB(pz)_3^-$. Upon addition of B, the red-brown heterogeneous Fe(III)–$MPDP^{2-}$ mixture gradually changed to the characteristic green solution of $[Fe_2O(MPDP)B_2Cl_2]$. Optical spectrophotometric examination of the crude reaction mixtures suggested that the desired dinuclear product was the major iron-containing species in solution. Attempts to isolate $[Fe_2O(O_2CR)_2B_2Cl_2]$ (R = CH_3, Ph) by using monocarboxylate anions in place of Na_2MPDP were unsuccessful. These assembly suntheses using $MPDP^{2-}$ thus provide a general synthetic route to $\{Fe_2O(MPDP)\}^{2+}$ complexes having a variety of terminal donor ligand types.

The green insoluble solids observed during the workup of the reaction mixtures suggests that polymerization to form heterogeneous iron–oxo–carboxylato complexes occurs in reactions with Na_2MPDP as with acetate. Little is known about the composition of such soluble species formed in organic solvents prior to the addition of nitrogen donors. Attempts to isolate them have afforded a beautiful array of tri-, tetra-, hexa-, octa-, and undecanuclear complexes.[7a] Iron–oxo–$MPDP^{2-}$ complexes are probably related to these compounds, although no attempt has been made to crystallize them. The modest yield of **3** indicates that use of Na_2MPDP is not a superior route to the synthesis of $[Fe_2O(O_2CR)_2\{HB(pz)_3\}_2]$ complexes. Under similar assembly conditions, **1** is isolated in slightly higher yields (~70%) along with $[Fe\{HB(pz)_3\}_2]^+$.[30] In principle, $MPDP^{2-}$ should form and stabilize dinuclear complexes better than acetate because of the chelate effect. The stability of the insoluble polymers formed in the presence of $MPDP^{2-}$ may offset this effect, however.

The merit of the $MPDP^{2-}$ ligand is demonstrated by the successful syntheses of **4**–**6** under assembly conditions that previously gave tetranuclear complexes with monocarboxylate anions.[10,11,13] The solubility and stability of the 4,4′-Me_2bpy and polyimidazolylmethane complexes are markedly different. Compound **4** is very soluble in halogenated and polar solvents such as DMSO, but dissolves and quickly decomposes in MeOH and H_2O. Solutions of **4** in CH_2Cl_2 change from green to red over time, eventually depositing crystals of $[\{Fe(4,4'\text{-}Me_2bpy)_2Cl\}_2O][Fe_2OCl_6]$.[14b] Although crude reaction mixtures of **5** and **6** are very soluble in halogenated solvents, the isolated products are only moderately so and deposit insoluble solids. Compounds **5** and **6** are more soluble and stable in MeOH.

Compounds **5** and **6** significantly augment the limited number of known dinuclear iron complexes with imidazole as the sole terminal nitrogen donor ligand.[15,31] In **6**, only two of the three imidazoles of the tridentate ligand, TMICMe, are coordinated to iron. The remaining coordination site is occupied by chloride. The same result is observed in a related reaction where the tridentate imidazole ligand TICMe was added to $FeCl_3 \cdot 6H_2O$, yielding *cis*-$[Fe(TICMe)_2Cl_2]Cl$ (**7**).[32]

Terminal Ligand Exchange Reactions. Compound **3** could also be obtained quantitatively by addition of 2 equiv of $KHB(pz)_3$ to **4** (eq 2). Both terminal ligands are replaced by $HB(pz)_3^-$,

$$[Fe_2O(MPDP)(4,4'\text{-}Me_2bpy)_2Cl_2] + 2KHB(pz)_3 \rightarrow \underset{\mathbf{4}}{} [Fe_2O(MPDP)\{HB(pz)_3\}_2] + 2KCl + 2(4,4'\text{-}Me_2bpy) \quad (2)$$
$$\underset{\mathbf{3}}{}$$

leaving the $[Fe_2O(MPDP)]^{2+}$ core unchanged. This ligand exchange reaction is related to those of the bridging carboxylate ligands in $[Fe_2O(O_2CCH_3)_2\{HB(pz)_3\}_2]$ (**1**), which led to the preparation of new complexes, including phosphate and phosphinate ester bridged compounds.[33] Conceivably, terminal ligand substitution reactions of **4** and **5** would have a similar synthetic utility.

(28) Rardin, R. L.; Tolman, W. B.; Lippard, S. J. *New. J. Chem.*, in press.
(29) (a) Toftlund, H.; Murray, K. S.; Zwack, P. R.; Taylor, L. F.; Anderson, O. P. *J. Chem. Soc., Chem. Commun.* **1986**, 191. (b) Wieghardt, K.; Tolksdorf, I.; Hermann, W. *Inorg. Chem.* **1985**, *24*, 1230. (c) Hartman, J. R.; Lippard, S. J. Unpublished results.
(30) Armstrong, W. H.; Lippard, S. J. Unpublished results.
(31) (a) Wu, F.-J.; Kurtz, D. M., Jr. *J. Am. Chem. Soc.* **1989**, *111*, 6563. (b) Gorun, S. M.; Papaefthymiou, G. C.; Frankel, R. B.; Lippard, S. J. *J. Am. Chem. Soc.* **1987**, *109*, 4244.
(32) Tolman, W. B.; Lippard, S. J. Unpublished results. X-ray crystallographic studies confirm the structure of *cis*-$[Fe(TICMe)_2Cl_2]Cl$.
(33) (a) Armstrong, W. H.; Lippard, S. J. *J. Am. Chem. Soc.* **1985**, *107*, 3730. (b) Turowski, P. N.; Armstrong, W. H.; Roth, M. E.; Lippard, S. J. *J. Am. Chem. Soc.* **1990**, *112*, 681.

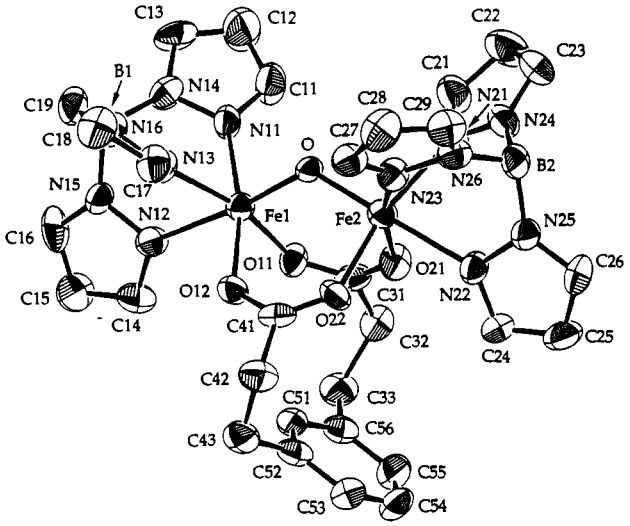

Figure 2. ORTEP drawing of $[Fe_2O(MPDP)\{HB(pz)_3\}_2]\cdot 5CHCl_3$ (**3**·$5CHCl_3$) showing 50% thermal ellipsoids and the atom-labeling scheme. Hydrogen atoms are omitted for clarity.

Chart I. Designation of Atom Labels Used in Tables II and III[a]

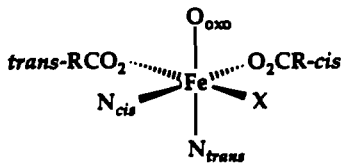

[a] $Fe-N_{cis/trans}$ designates iron–nitrogen bonds situated, respectively, cis or trans to the bridging oxo ligand. $Fe-O_2CR$-*cis*/*trans* designates a carboxylate oxygen atom positioned adjacent or opposite to a terminal chloride or, for $metN_3myoHr$, the terminal azide. For **1** and **3**, O_2CR-*cis*/*trans* are the same and X is equal to N_{cis}. X is defined as nitrogen for **1** and **3** or as an anion for **2**, **4**, **5**, and $metN_3myoHr$.

Structural Studies. The molecular structure of **3**, displayed in Figure 2, consists of two six-coordinate iron atoms bridged by an oxo group and two carboxylato ligands with two facially coordinating tridentate $HB(pz)_3^-$ ligands in the terminal positions. This coordination environment is analogous to that of iron coordinated by the three terminal histidine ligands in Hr. The coordination geometries of **1** and **3** are nearly identical, as shown in Tables II and III. The pseudo-2-fold symmetry in the structure of **1** is not preserved in **3**, which has only C_s symmetry owing to coordination of the $MPDP^{2-}$ ligand. Both complexes are tetragonally distorted as a result of the short $Fe-O_{oxo}$ bond[8] (Table II and Chart I). The short $Fe-O_{oxo}$ bonds in **1** and **3** lengthen the trans Fe–N distances as observed for numerous other $\{Fe_2O(O_2CR)_2\}^{2+}$ complexes[7] and $metN_3myoHr$.[6a]

The structure of **3** illustrates how the $MPDP^{2-}$ ligand spans the dinuclear core. The carboxylate ligand geometry in **3** is essentially unperturbed compared to that in **1**, although slightly more skewed. This distortion can be quantitated by computing the maximum deviation of an iron atom from the least-squares plane defined by the four atoms in the $C-CO_2^-$ unit, which is larger in **3** (0.26 Å) than in **1** (0.15 Å). The distance between α-methylene carbon atoms in **3** (5.9 Å) is similar to the $CH_3\cdots CH_3$ separation in **1** (6.0 Å). This result confirms that the new ligand can adopt a configuration that permits carboxylates to bridge the dinuclear iron center as in **1**.

The coordination of the $MPDP^{2-}$ ligand to the $\{Fe_2O\}^{4+}$ core in the $[Fe_2O(MPDP)B_2Cl_2]$ complexes is essentially the same, as illustrated in Figures 3 and 4. The terminal coordination sites, however, are now occupied by bidentate ligands, with one nitrogen cis and the other trans to the bridging oxo atom. The remaining terminal coordination site on each iron atom contains a chloride cis to this group. With the change in terminal donor set from NNN to NNCl, the structures of **4** and **5** have no symmetry, all Fe–ligand bonds in the complexes being unique. Unlike the iron

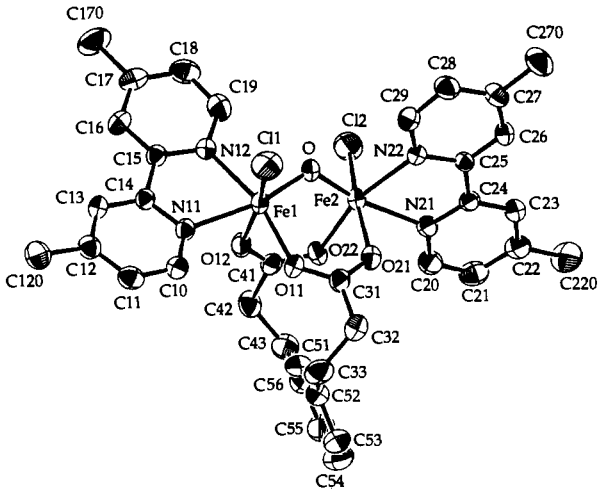

Figure 3. ORTEP drawing of $[Fe_2O(MPDP)(4,4'\text{-}Me_2bpy)_2Cl_2]\cdot 2CH_3CN$ (**4**·$2CH_3CN$) showing 50% thermal ellipsoids and the atom-labeling scheme. Hydrogen atoms are omitted for clarity.

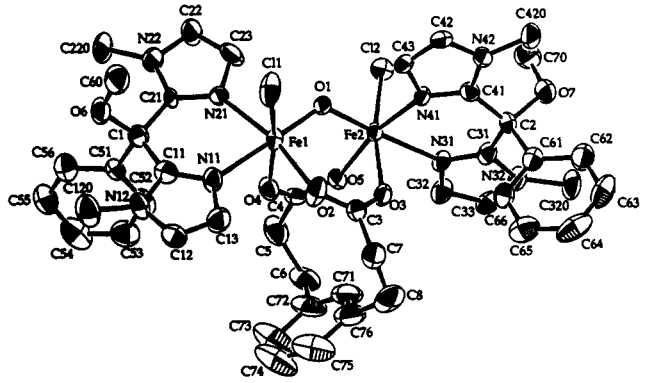

Figure 4. ORTEP drawing of $[Fe_2O(MPDP)(BIPhMe)_2Cl_2]\cdot 3CHCl_3\cdot CH_3CN$ (**5**·$3CHCl_3$·CH_3CN) showing 65% thermal ellipsoids and the atom-labeling scheme. Hydrogen atoms are omitted for clarity.

atoms in **3**, those in **4** and **5** are analogous to the Fe center in Hr that binds exogenous ligands and dioxygen (as hydroperoxide). The two chloride atoms in **4** and **5** are arranged such that the Cl1–Fe1–Fe2–Cl2 torsion angles are 81.9 (2) and 80.0 (3)°, respectively, which we define as the anti configuration. This configuration is also observed in **2** (Cl–Fe1–Fe2–Cl = 82.3 (2)°).[12] The carboxylate oxygen atoms trans to chloride are all slightly longer than the cis oxygen atoms (Chart I, Table III), reflecting the trans-directing influence of Cl^-. A similar lengthening of carboxylate oxygen trans to the N_3^- ion occurs in the structure of $metN_3myoHr$.[6a]

Examination of Table III allows several comparisons to be made among the structures of **1**–**5**, $metN_3myoHr$, and related complexes. The Fe–Cl distances are somewhat longer than those of other octahedral high-spin iron(III) complexes,[34] partly due to greater steric interactions among bridging ligands in the core and partly because of the fact that the oxo and nitrogen atom donors diminish the electrophilicity of the iron center. The longer Fe–Cl bonds observed in **5** versus **2** and **4** may be the result of tighter binding of imidazole (Fe–N average, 2.141 (6) Å) compared with pyridine (Fe–N average, 2.181 (4) Å). The average Fe–N distances in **5** appear to be somewhat shorter than the 2.19 Å value in $metN_3myoHr$.[6a] It is noteworthy that there is little difference

(34) Comparative Fe–Cl bond lengths are as follows. (a) $[Fe_2L(OCH_3)Cl_2]$ (2.317 (7) Å and $[Fe_2L(OH)Cl_2]$ (2.30 (1) Å L = trisalicylidenetriethylenetetraamine: Chiari, B.; Piovesana, O.; Tarantelli, T.; Zanazzi, P. F. *Inorg. Chem.* **1983**, *22*, 2781. (b) $[Fe_3(TIEO)_2(O_2CPh)_2Cl_3]$ (2.276 (3) Å).[31b] (c) $[(Fe(phen)_2Cl)_2O]Cl_2$ (2.34 (1) Å): Healy, P. C.; Skelton, B. W.; White, A. H. *Aust. J. Chem.* **1983**, *36*, 2057. (d) $[Fe(bpy)_2Cl_2]FeCl_4$ (2.254 (2) Å): Skelton, B. W.; White, A. H.; Figgis, B. N.; Patrick, J. M.; Reynolds, P. A.; Healy, P. C. *Aust. J. Chem.* **1983**, *36*, 2043.

Table IV. Comparison of Electronic and Vibrational Properties of **1**–**6** and Hr

	1	**2**	**3**	**4**	**5**	**6**	$metN_3Hr$	metClHr
				Electronic Spectral Data (λ_{max}, nm (ϵ, cm^{-1} mol^{-1} L^{-1}))[a]				
LMCT[b]	339 (4635)	329 (6060)	341 (4600)	328 sh	341 (3000)	335 (3220)	326 (3375)	329 (3030)[c]
$O^{2-} \rightarrow$ Fe CT, LMCT[b]	358 sh		365 (sh)	365 sh	360 sh	356 sh	380 sh (2150)	380 sh (3000)
$^6A_1 \rightarrow [^4T_2](^4D)$[b]	457 (505)	464 sh (387)	460 (440)	462 (450)		475 (380)	446 (1850)	
$^6A_1 \rightarrow [^4A_1,^4E](^4G)$[b]	492 (460)		493 (400)	483 (400)	483 (400)	485 (350)		490 sh (375)
$O^{2-} \rightarrow$ Fe CT[d]	528 sh		533 (sh)	535 sh	525 sh	530 sh	530 sh	656 (90)
$^6A_1 \rightarrow [^4T_2](^4G)$[e]	695 (70)		698 (60)	655 (70)	682 (90)	684 (60)	680 (95)	1020 (5.5)
$^6A_1 \rightarrow [^4T_1](^4G)$[e]	995 (3.5)		*f*	950 (4.3)	1020 (2.2) (CH_3OH)	*f*	1010 (5.1)	
				Vibrational Data (cm^{-1})[g]				
ν_s(Fe–O–Fe)	528	*f*	526	532	522	524	507	509[h]

[a] Reported for $CHCl_3$ (**1**, **3**, **5**, and **6**) and CH_2Cl_2 (**2**[12] and **4**) solutions. [b] Reference 37c. [c] References 37c and 40. [d] References 37c, 39, and 36b. [e] References 8, 9, 36, 37, and 39. [f] Not measured. [g] Spectra of **1**,[8] **3**, **5**, and **6** in $CHCl_3$ and **4** in CH_2Cl_2 were collected with 514.5-nm Ar^+ laser excitation. [h] References 5 and 40.

between Fe–N bond lengths in high-spin Fe(III)–imidazole and –1-methylimidazole complexes, the 2.135 Å average Fe–N distance of the imidazole complex $[Fe(HTIEO)(TIEO)]^{2+}$ also being rather short.[31b] Differences between the BIPhMe and dipyridine ligands are manifest in the N–Fe–N angles, the smaller bite angle in **4** resulting in larger deviations from ideal geometry in this structure. The larger Fe–O–Fe angle of the imidazole complex most closely approaches the 130° value observed in the structure of $metN_3myoHr$.[6a] Comparison of the structures of **2** and **4** reveals similar bond lengths and angles. The Fe–O distance of 1.773 (4) Å in **4** is the shortest reported and diminishes the nonbonded Fe···Fe distance. These differences may be ascribed to different conformational geometries of the coordinated $MPDP^{2-}$ ligand, described below.

Conformation of the Dicarboxylate Ligand. The conformational flexibility of the $MPDP^{2-}$ phenyl ring and its methylene linkers with respect to the $\{Fe_2O\}^{4+}$ core is illustrated in Figure 5a, where the structures of **3**–**5** are viewed perpendicular to the plane defined by the Fe–O_{oxo}–Fe atoms. We define the tilt (τ) of the phenyl ring to be the dihedral angle between the best mean planes through its six carbon atoms and those of the four carboxylate oxygen atoms, both shown in the accompanying diagram, Figure 5b. The τ values for **3**–**5** are given in Figure 5a.

In compounds **3** and **5**, the methylene chains fold back over the phenyl ring such that the C_α–C_β bonds eclipse one another. In the case of **4**, the methylene chains are staggered. In addition to producing a τ value (64°) of greater magnitude than the eclipsed conformation, this configuration causes significant twisting of the carboxylate groups relative to the Fe···Fe vector. This twist is reflected by large deviations (maximum value, 0.49 Å) of the iron atoms from the least-squares planes defined by the C–CO_2^- carboxylate groups. The β-CH_2–β-CH_2 distance of 5.5 Å for the $MPDP^{2-}$ ligand in **4** also reflects this distortion, being slightly under the 5.7–6.0-Å range found in the other complexes. The Fe–O carboxylate bond length trans to the chloride anion in **4** is greater than in **2**, 2.177 (4) vs 2.109 (5) Å, respectively, possibly due to poor Fe–$O_{CO_2^-}$ bond orbital overlap because of the twist.

Interestingly, the cis and trans Fe–$O_{CO_2^-}$ bond lengths in **4** are nearly identical with those found in $metN_3myoHr$.[6a] Although a large number of model complexes with a variety of terminal ligands have been structurally characterized, average metal–ligand bond lengths in the proteins remain significantly larger by comparison. It has been suggested that these differences could be due to structural constraints imposed by the polypeptide backbone or to an error in the structure determination.[35] The lengthening of the Fe–$O_{CO_2^-}$ bond distances in **4** due to ligand conformational effects represents an example of the consequences of such a structural constraint.

Electronic and Vibrational Spectroscopic Properties. Electronic spectral data and assignments for compound **3**–**6** are listed in Table IV, along with results for **1**, **2**, and metHr derivatives for comparison purposes. The energies of bands in the optical and vibrational spectra of **3** are nearly identical with those of **1** and are characteristic of $\{Fe_2O(O_2CR)_2\}^{2+}$ complexes.[8,9,36a] The spectra of **4**–**6** are similar to those of **2** and metClHr,[37] which are not unlike that of **1**. This result is consistent with the coordination of chloride ion, which produces little or no charge-transfer transitions in the exogenous LMCT region (400–550 nm).[37c] Shoulders in the iron–oxo spectral region (300–400 nm) of complexes **2** and **4** resolve into peaks in **5** and **6**. Intense dipyridine MLCT UV transitions in **2** and **4** partially obscure the iron–oxo transitions. The spectra of **2** and **4** are similar, although several bands present in **4** were not previously reported for **2**.[12]

On the basis of their relative positions, the low-energy ligand field bands (550–850 nm) of metMHr have been correlated with the ligand field strength of the exogenous monodentate ligand, M.[37c] An analogous effect is observed for terminal ligand sets of **3**–**5**, specified here in order of decreasing ligand field strength: N3(pyrazole) (698 nm) > N2(imidazole)Cl (682 nm) > N2(pyridine)Cl (655 nm). These results are consistent with chloride being a weaker field ligand than heterocyclic nitrogen and the

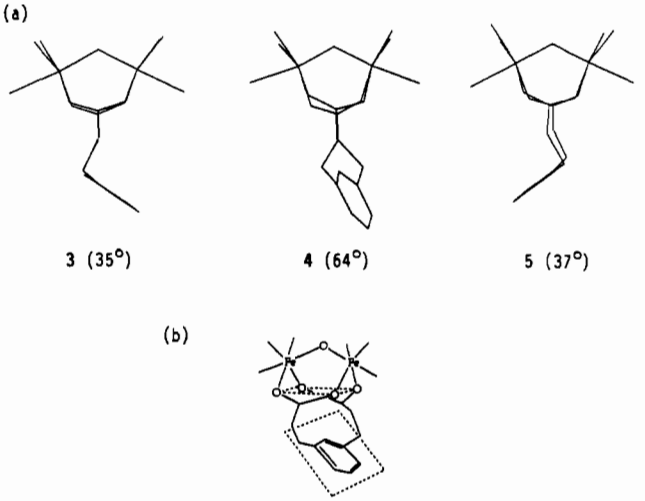

Figure 5. (a) View of **3**–**5** perpendicular to the plane formed by the Fe–O–Fe atoms that shows the staggered (**4**) and eclipsed (**3** and **5**) methylene chains and the tilt, τ (deg, in parentheses), of the $MPDP^{2-}$ phenyl ring. (b) Diagram depicting the tilt angle, τ, the dihedral angle formed between planes defined by the carboxylate oxygen atoms, and the $MPDP^{2-}$ phenyl ring.

(35) Stenkamp, R. E.; Sieker, L. C.; Jensen, L. H. *Acta Crystallogr.* **1983**, *B39*, 697.

(36) (a) Spool, A.; Williams, I. D.; Lippard, S. J. *Inorg. Chem.* **1985**, *24*, 2156. (b) Czernuszewicz, R. S.; Sheats, J. E.; Spiro, T. G. *Inorg. Chem.* **1987**, *26*, 2063.

(37) (a) Garbett, K.; Darnall, D. W.; Klotz, I. M.; Williams, R. J. P. *Arch. Biochem. Biophys.* **1969**, *103*, 419. (b) Garbett, K.; Johnson, C. E.; Klotz, I. M.; Okamura, M. Y.; Williams, R. J. P. *Arch. Biochem. Biophys.* **1971**, *142*, 574. (c) Reem, R. C.; McCormick, J. M.; Richardson, D. E.; Devlin, F. J.; Stephens, P. J.; Musselman, R. L.; Solomon, E. I. *J. Am. Chem. Soc.* **1989**, *111*, 4688. (d) Norman, R. E.; Holz, R. C.; Menage, S.; O'Connor, C. J.; Zhang, J. H.; Que, L., Jr. *Inorg. Chem.* **1990**, *29*, 4629. (e) Butcher, K. D.; Gebhard, M. J.; Solomon, E. I. *Inorg. Chem.* **1990**, *29*, 2067.

tighter binding of imidazole than dipyridine to the $\{Fe_2O(O_2CCH_3)_2\}^{2+}$ core. In the formate analogue of **6**, $[Fe_2O(O_2CH)_4(BIPhMe)_2]$, the corresponding band is found at 662 nm,[15] implying that formate is a weaker field ligand than chloride. The fact that the ligand field bands of **5** and **6** are virtually identical confirms that **6** has a terminal chloride rather than imidazole coordinated to iron.

The $^6A_1 \rightarrow {}^4T_2$ ligand field transition in metClHr occurs at 656 nm and is an average of two bands expected for the NNCl and NNN donor sets.[37a,c] This transition occurs at the same energy as in **4**, which has two NNCl donor atom sets. These results suggest that the ligand field strength is weaker in the protein than in the polyimidazole ligands studies here, which is consistent with the longer Fe–N bond distances found in structural studies of metHr.[6] It is interesting that model complexes having a NNCl terminal donor set more closely match the smaller extinction coefficients found in the iron–oxo region of metMHr derivatives than complexes with a NNN donor set.[37a-c] Thus, although the electronic spectra are dominated by the $\{Fe_2O(O_2CCH_3)_2\}^{2+}$ core, the type and strength of terminal ligand binding can shift the low-energy ligand field bands and affect extinction coefficients in the iron–oxo region.[33b]

The lowest energy ligand field band occurs in the near-IR region (850–1200 nm) and is also sensitive to changes in terminal ligands.[33b,37c,38] A broad, weak absorption is observed at 950 nm for **4** in CH_2Cl_2 and 1020 nm for **5** in MeOH. In **3**, this band appears at 995 nm in $CHCl_3$. The energy and intensity of these absorbances compare well with those at 1020 nm for metClHr and 1010 nm for $metN_3Hr$.[37c,38] From the positions of these near-IR bands alone, the relative ligand field strengths vary according to N2(imidazole)Cl > N3(pyrazole) > N2(pyridine)Cl. These trends to not match those for the higher energy ($^4T_2$) ligand field transition (550–850 nm) in either the protein or the model complexes. From a study of a series of dinuclear iron–oxo model complexes it was concluded that the spectral bands in the 550–800-nm region may be dominated by forbidden oxo LMCT transitions rather than by ligand field effects.[37d] Charge-transfer modulation of the ligand field bands[37e] could also be a factor (cf. also the discussion in ref 15b).

Compounds **3–6** all display a strong, resonance-enhanced Fe–O–Fe symmetric stretch. The bands vary from 522 to 532 cm^{-1} and fall within the narrow range of frequencies observed for most $\{Fe_2O(O_2CR)_2\}^{2+}$ centers and proteins (486–540 cm^{-1}).[36,39] The variational frequency of the symmetric stretch can be calculated from eq 3, derived from an empirical correlation between the

$$\nu_s^2\ (cm^{-2}) = 4.252 \times 10^5 + 2.826 \times 10^5 \cos \phi \qquad (3)$$

Fe–O–Fe vibrational frequency, ν_s, and the Fe–O–Fe angle, ϕ.[33b] The observed ϕ (123.4°) and ν_s (526 cm^{-1}) values of **3** agree well with the calculated ones (122.3° and 524 cm^{-1}). Similarly, the larger 135° Fe–O–Fe angle in $metN_3myoHr$ results in a smaller vibrational frequency (507 cm^{-1}).[10,40] Slightly lower frequency bands occur in the polyimidazole complexes (522–524 cm^{-1}) compared to **3** (526 cm^{-1}) and **4** (532 cm^{-1}). The low-energy frequency shifts observed for **5** and $metN_3Hr$ versus those observed for **3** and **4** are consistent with the increase in the Fe–O–Fe angles established by structural studies. From the observed frequency of compound **6** (524 cm^{-1}) and metClHr (509 cm^{-1}),[40] for which no crystal structure has been determined, eq 3 predicts $\phi = 122°$ for **6** and $\phi = 126°$ for metClHr.

Interestingly, under the conditions of the resonance Raman experiment, compound **4** undergoes photodecomposition. No such decomposition occurs for **5** and **6**, indicating that the dipyridine ligand photosensitizes **4**. Although no photochemistry has been previously reported for $\{Fe_2O(O_2CCH_3)_2\}^{2+}$ complexes, several photochemical reactions have been observed in MMO (photoreduction),[3c,41] RR,[42] and Hr (ligand substitution).[43]

Table V. Comparison of Magnetic and Mössbauer properties of **1–6** and Hr

	1[a]	**2**[b]	**3**	**4**	**5**	**6**	Hr
			Magnetic Data[c]				
$-J$, cm^{-1}	121	132	125	119	122	124	134 (metHr)[d]
			Mössbauer Data[e]				
δ, mm s^{-1}	0.52	0.37	0.53	0.51	0.52	0.54	0.59 (metClHr)[f] 0.50 ($metN_3Hr$)[f]
ΔE_Q, mm s^{-1}	1.60	1.80	1.66	1.66	1.94	1.78	2.12 (metClHr) 1.90 ($metN_3Hr$)

[a] Reference 8. [b] Reference 12. [c] Magnetic measurements and analyses were performed as described in text. [d] Reference 45. [e] Mössbauer parameters were obtained at 4.2 K. [f] Reference 37b.

Magnetic and Mössbauer Data. Variable-temperature solid-state magnetic susceptibility measurements were performed on powdered samples of **3–6**. The Heisenberg–Dirac–van Vleck model for magnetic coupling in a dinuclear complex was used to interpret the temperature dependence of the magnetism.[26,44] Data were fit by using a susceptibility expression derived from the spin-exchange Hamiltonian, $H = -2J\mathbf{S}_1\cdot\mathbf{S}_2$ ($S_1 = S_2 = {}^5/_2$), where J is the spin exchange coupling constant, as described previously.[8,9] Additional terms for temperature-independent paramagnetism, TIP, and a mole percentage of paramagnetic impurity, p, were included in the susceptibility expression. The best least squares fit for **3** gave $J = -124.6$ (4) cm^{-1}, $p = 0.47\%$, and TIP = 208 $\times 10^{-6}$ cgsu mol^{-1} with a correlation coefficient of 0.9995. The antiferromagnetic coupling constant for **3** was close to that of **1** (−121.3 (1) cm^{-1}) obtained with a similar fitting procedure.[8] The best least squares fit for **4** gave $J = -118.5$ (2) cm^{-1}, $p = 0.34\%$, and TIP = 198 $\times 10^{-6}$ cgsu mol^{-1} with a correlation coefficient of 0.9999. The best least-squares fits for **5** and **6**, respectively, gave $J = -121.5$ (3) and −123.9 (4) cm^{-1}, $p = 0.15\%$ and 0.33%, and TIP = 143 $\times 10^{-6}$ and 212 $\times 10^{-6}$ cgsu mol^{-1} with correlation coefficients of 0.9997 and 0.9996.

The antiferromagnetic coupling constants of **3–6** fall within the range found for most multiply bridged diiron(III)–oxo compounds and metHr (Table V).[7,45] The J values for **4–6** and the protein are similar to those obtained for **1** (−121 cm^{-1}) and **3** (−125 cm^{-1}), which have tridentate terminal nitrogen donors. Clearly, the degree of antiferromagnetic coupling is not significantly affected by changing nitrogen donors or substituting of Cl for N in the terminal positions of the $\{Fe_2O(O_2CR)_2\}^{2+}$ core. In contrast, protonation of the oxo bridge diminishes J by an order of magnitude,[33a] consistent with the oxo ligand being the main magnetic exchange pathway.

The coupling constants for **2** and **4** differ by 13 cm^{-1}, a variation that may arise in part from differences in the way in which the data were acquired and analyzed. In the fit of the data for **4**, g was fixed at 2.0, a reasonable assumption in the case of high-spin Fe(III), which has a nondegenerate $^6A_1$ ground state.[26b] Use of a TIP term improved calculated fits significantly in the 20–80 K temperature range, where the magnetic susceptibility reaches a minimum. Omitting a TIP term gave consistently lower values for J. Replacing the TIP correction with a Curie–Weiss term, Θ, where $\chi = C/(T + \Theta)$, did not significantly improve the fit. Although it was unnecessary to vary g for compound **4**, **2** was best fit by varying g (optimized to 1.90) and with the inclusion of a TIP term (optimized to 800 $\times 10^{-6}$ cgsu mol^{-1}).[12]

Table V summarizes results for single-site least-squares fits of the 4.2 K Mössbauer data for compounds **3–6**. The isomer shifts

(38) Sanders-Loehr, J.; Loehr, T. M.; Mauk, A. G.; Gray, H. B. *J. Am. Chem. Soc.* **1980**, *102*, 6992.
(39) Sanders-Loehr, J.; Wheeler, W. D.; Shiemke, A. K.; Averill, B. A.; Loehr, T. M. *J. Am. Chem. Soc.* **1989**, *111*, 8084.
(40) Freier, S. M.; Duff, L. L.; Shriver, D. F.; Klotz, I. M. *Arch. Biochem. Biophys.* **1980**, *205*, 449.
(41) DeWitt, J. G.; Bentsen, J. G.; Rosenzweig, A. C.; Hedman, B.; Green, J.; Pilkington, S.; Papaefthymiou, G. C.; Dalton, H.; Hodgson, K. O.; Lippard, S. J. Submitted for publication.
(42) Backes, G.; Sahlin, M.; Sjöberg, B.-M.; Loehr, T. M.; Sanders-Loehr, J. *Biochemistry* **1989**, *28*, 1923.
(43) Duff, L. L.; Klippenstein, G. L.; Shriver, D. F.; Klotz, I. M. *Proc. Natl. Acad. Sci. U.S.A.* **1981**, *78*, 4138.
(44) Murray, K. S. *Coord. Chem. Rev.* **1974**, *12*, 1.
(45) Dawson, J. W.; Gray, H. B.; Hoenig, H. E.; Rossman, G. R.; Schredder, J. M.; Wang, R. H. *Biochemistry* **1972**, *11*, 461.

Table VI. Summary of ^{1}H NMR Spectral Data and T_1 Values for **1**, **3**–**6**, $[Fe_2O(O_2CCH_3)_2(TMIP)_2]^{2+}$, and metClHr[a]

1	3	4	5	6	$[Fe_2O(O_2CCH_3)_2(TMIP)_2]^{2+}$ [b]	metClHr[c]
$HB(pz)_3^-$	$HB(pz)_3^-$	4,4′-Me_2bpy	BIPhMe	TMICMe	TMIP	histidine
12.1 (2.7) [H4,H5]	13.0 (1.6) [H4,H5]	16.1 (0.4) [H6]	13.0 (1.5) [H5]	13.0 [H5]	13.9, 11.3 [H5]	23, 19, 13 [NH]
9.1 (0.3) [H3]	*d*	13.9 (1.0) [H3]				
		12.5 (0.8) [H5]				
2.5 (1.2) [BH]	3.0 (0.8) [BH]		7.4 (5.0) [Ph]			
		2.9 (4.0) [4-CH_3]	5.3 (3.0) [*N*-CH_3]	5.3 [*N*-CH_3]	5.1, 4.6 [*N*-CH_3]	
			3.4 (1.5) [*O*-CH_3]			
$CH_3CO_2^-$	$MPDP^{2-}$	$MPDP^{2-}$	$MPDP^{2-}$	$MPDP^{2-}$	$CH_3CO_2^-$	Asp/Glu
10.5 (1.1)	10.9 (1.3) [α-CH_2]	10.9 (1.3) [α-CH_2]	10.5 (0.6) [α-CH_2]	10.6 [α-CH_2]	10.1 [CH_3]	11 [α-CH_2]
	7.4 (4.5) [Ph]	7.0 (3.0) [Ph]	7.4 (5.0) [Ph]	7.2 [Ph]		
	5.5 (1.1) [β-CH_2]	4.6 (2) [β-CH_2]	5.0 [β-CH_2][e]	5.0 [β-CH_2][e]		

[a] Shifts are in ppm downfield of TMS, T_1 values in ms are given in parentheses, and assignments are given in square brackets. A diagram of the ligands, their abbreviations, and their atom-numbering schemes are given in Chart II. The spectra were obtained for solutions of **1** in CD_2Cl_2, for solutions **3** and **4** in $CDCl_3$, for solutions **5** and **6** in CD_3OD, and for solutions **7** and **8** in CD_3CN. [b] Reference 31a. [c] Reference 48. [d] H3 is not observed. [e] Overlaps the solvent resonance.

(δ) fall in the 0.46–0.52 mm s^{-1} range of most other $\{Fe_2O(O_2CCR)_2\}^{2+}$ complexes.[7] The isomer shift of **3** (0.53 mm s^{-1}) compares well with that of **1** (0.52 mm s^{-1}) and agrees with expectations from measurements made on a large variety of mononuclear and oxo-bridged dinuclear Fe(III) complexes.[7e,44,46] Inexplicably, the isomer shifts of **2** and **4** differ greatly, 0.37 vs 0.51 mm s^{-1}, respectively.

Although the quadrupolar splitting (ΔE_Q) in **3** is in close agreement with that of **1**, a larger range of values occurs for **3**–**6** (1.66–1.94 mm s^{-1}). There are also significant differences between **2** and **4** (1.80 vs 1.66 mm s^{-1}, respectively). The electric field gradient responsible for changes in the quadrupole splitting is most affected by the short Fe–O_{oxo} bond vector. Additional asymmetry in the electronic environment of the iron coordination sphere caused by tighter binding of the imidazole nitrogen donor trans to the oxo ligand and a weaker Fe–Cl interaction could increase the quadrupole splitting in the polyimidazole complexes. The splitting observed in **5** is the largest reported among the model complexes of diiron(III)–oxo proteins, approaching the value for metClHr (2.12 mm s^{-1}).[37a] Reasons for variations in the quadrupole coupling constants of the protein diiron(III)–oxo centers and models have been difficult to discern, and a larger body of data may be required before any conclusive interpretations can be made.

Electrochemistry. The cyclic voltammogram of **3** exhibits a large cathodic wave at −895 mV vs Ag/AgCl. This behavior is similar to that of **1**, which undergoes an irreversible reduction at −760 mV vs SCE in acetonitrile.[8] The products of the reduction of **3** are $[Fe\{HB(pz)_3\}_2]$ ($E_{1/2}$ = 220 mV), which is also observed for **1**, and other electrochemically active species (E_a = −805 mV, E_a = −595 mV, and E_a = −95 mV) not observed in **1**. Limiting the scan range allows a reversible couple having $E_{1/2}$ = −133 mV, corresponding to the unidentified species with E_a = −95 mV, to be observed. This species could be an electrochemically active Fe–MPDP complex, formed upon reductive decomposition of **3**, but no attempt was made to isolate it. An anodic scan reveals an oxidation at E_a = 1600 mV that leads to formation of $[Fe\{HB(pz)_3\}_2]^+$. Generation of $[Fe\{HB(pz)_3\}_2]$ in the cyclic voltammetry of **3** demonstrates that linking the carboxylates of the $\{Fe_2O(O_2CR)_2\}^{2+}$ core does not prevent reductive or oxidative decomposition. Moreover, in contrast to **1**, repetitive scans of **3** do not reproduce the first scan; rather, they suggest deposition of solids on the electrode.

Compounds **4**–**6** partially decomposed under the high ionic strength conditions of the electrochemical experiment, as revealed by optical spectrophotometry. Compound **4** underwent substantial decomposition, whereas **5** and **6** were more stable. Cyclic voltammetry of **4** revealed a large irreversible wave at −745 mV that generated new waves on the return cycle owing to reductive decomposition. The behavior of **5** and **6** was similar. Oxidation of free chloride ion was observed, as noted earlier for **2** (E_c ranging from ~1300 to 1500 mV vs Ag/AgCl),[10] and in the case of **4**, the $[Fe(4,4'\text{-}Me_2bpy)_3]^{2+/3+}$ couple ($E_{1/2}$ = 1.13 V vs Ag/AgCl) was detected.

Chart II. Diagram of the Nitrogen and Oxygen Ligands Presented in this Work Along with Their Abbreviations and Atom-Numbering Scheme

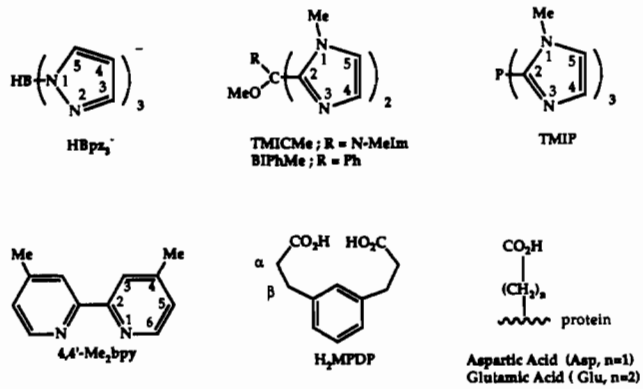

^{1}H NMR Spectroscopy. Paramagnetically shifted ^{1}H NMR resonances and spin–lattice relaxation times (T_1) of compounds **3**–**6** are listed in Table VI, and an accompanying diagram of the ligands is presented in Chart II. All resonances fall in the 0–20 ppm range, the strong antiferromagnetic coupling in $\{Fe_2O(MPDP)\}^{2+}$ complexes reducing the magnetic moment to ~1.8 μ_B per Fe and resulting in small positive isotropic shifts that are contact in origin.[7]

With the exception of additional resonances due to the $MPDP^{2-}$ β-methylene and phenyl ring protons, the spectrum of **3** is very similar to that of **1**. The pyrazole ring H4 and H5 protons appear as a single resonance at 13.0 ppm, but H3 is not observed. The H3 resonance in **1** is a very broad line centered at 9.1 ppm and has the smallest T_1 value, consistent with its close proximity to the paramagnetic Fe center.[47] The $MPDP^{2-}$ ligand resonances occur at 10.4 (α-methylene), 7.4 (phenyl), and 5.5 (β-methylene) ppm. The T_1 values are fairly similar to those in **1**. Paramagnetically shifted resonances in Hr at 11 ppm have been tentatively assigned to methylene protons of coordinated aspartic and glutamic acid residues, but no T_1 measurements were reported.[48] In **1** and **3**, these resonances occur at 10.5 and 10.9 ppm, respectively, underscoring the value of these complexes as spectroscopic models for the dinuclear iron–oxo center in Hr. Although RR has a

(46) Gibb, T. C.; Greenwood, N. N. In *Mössbauer Spectroscopy*; Chapman and Hall: London, 1971; pp 148–164.

(47) Swift, T. J. In *NMR of Paramagnetic Molecules*; La Mar, G. N., Horrocks, W. DeW., Jr., Holm, R. H., Eds.; Academic Press: New York, 1973; p 53.

(48) Maroney, M. J.; Kurtz, D. M., Jr.; Nocek, J. M.; Pearce, L. L.; Que, L., Jr. *J. Am. Chem. Soc.* **1986**, *108*, 6871.

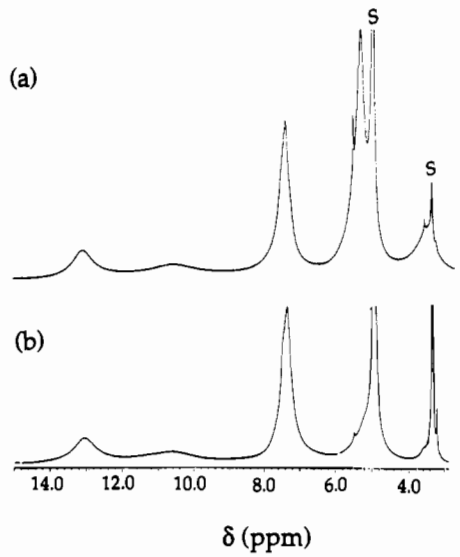

Figure 6. ^{1}H NMR specta of (1) $[Fe_2O(MPDP)(BIPhMe)_2Cl_2]$ (**4**) and (b) the deuterated derivative $[Fe_2O(MPDP)(BIPhMe\text{-}d_9)_2Cl_2]$ in CD_3OD. The peaks labeled S are due to solvent.

carboxylate-bridged core, this region of the ^{1}H NMR spectrum is obscured by other protein resonances.[49]

Three broad downfield resonances in **4** are assigned to the three dipyridine ring protons. A total of six such resonances is expected, as a result of cis and trans dispositions of each ring with respect to the Fe–O_{oxo} bond, but these lines are not resolved in the spectrum. Despite having similar magnetic moments, resonances in the dipyridine complex are shifted farther downfield than in the corresponding pyrazolyl compound, **3**, owing to the greater aromaticity of pyridine. A comparable trend in shifts occurs in the ^{1}H NMR resonances of nitrogen donors of $\{Fe_4O_2(O_2CPh)_7B_2\}$ complexes (B = H_2Bpz_2 (17.1–12.5 ppm) vs 4,4′-Me_2bpy (22.7–16.1 ppm).[11a] On the basis of T_1 measurements, the resonance at 16.1 ppm is assigned to the H6 ring proton, which is situated closest to the iron center. The 13.9 and 12.5 ppm peaks were assigned to the H3 and H5 resonances based on their relative positions on the free ligand. The 4,4′-Me_2bpy methyl protons appear at 2.9 ppm. Assignment of the $MPDP^{2-}$ resonances in **2** assisted in the identification of resonances in compound **4**. The α-methylene protons of the $MPDP^{2-}$ ligand occur at 10.9 ppm in **4**, and the $MPDP^{2-}$ phenyl protons, at 7.0 ppm. A broad resonance at 4.6 ppm is assigned to the β-methylene protons. The spectrum of **4** contains features characteristic of dissociated 4,4′-Me_2bpy, including several sharp 4,4′-Me_2bpy ring proton resonances at 8.46, 8.15, and 7.05 ppm and, further upfield, a free pyridyl methyl group signal at 2.36 ppm. The presence of the free ligand is in contrast to the behavior of **3** and other $\{Fe_2O(O_2CR)_2\}^{2+}$ complexes, which are more stable in solution.

The spectra of **5** and its *N*-CD_3 and *O*-CD_3 deuterated derivatives (Table VI, Figure 6) reveal a single peak at 13.0 ppm assigned to the H5 proton, indicating that both cis and trans imidazole rings are effectively equivalent. The H4 resonance is too broad to be observed, as noted previously.[31a] The α-methylene protons of the $MPDP^{2-}$ ligand occur at 10.5 ppm. A broad peak with several shoulders at 7.4 ppm is attributed to the phenyl ring protons of both BIPhMe and $MPDP^{2-}$. These resonances have similar relaxation times, and a broad underlying resonance with a T_1 value of ~1.5 ms was observed at 7.4 ppm. The *N*-CH_3 peak appears as a singlet at 5.3 ppm, as confirmed by its absence in the deuterated derivative. In this deuterated analogue a broad, weak resonance appears at 5.0 ppm and is assigned to the β-methylene protons of the $MPDP^{2-}$ ligand. The broad resonance at 3.4 ppm assigned to the *O*-CH_3 proton resonances also disappears upon deuteration. Some dissociated BIPhMe, although less than in the case of **4**, is evident from the appearance of small, sharp resonances due to *N*-CH_3 and *O*-CH_3 groups. The spectrum of **6** displays resonances due to the same coordinated donors as observed for **5**, but also contains sharp phenyl, *N*-CH_3, and *O*-CH_3 resonances arising from the noncoordinating imidazole ring of TMICMe.

Recently, the ^{1}H NMR spectra of imidazole ligands coordinated to paramagnetic high-spin Fe(III) have been analyzed.[31a] The ^{1}H NMR resonances of $[Fe_2O(O_2CCH_3)_2(TMIP)_2]^{2+}$ and metClHr are also given in Table VI for comparison with those of **3**–**6**. In contrast to those of **5** and **6**, the spectrum of $[Fe_2O(O_2CCH_3)_2(TMIP)_2]^{2+}$ displays two sets of imidazole H5 and *N*-CH_3 resonances, at 13.9 and 11.3 ppm and 5.1 and 4.6 ppm, respectively. This result reflects the inequivalence of the trans (most downfield shifted) and cis positions of the imidazole rings relative to the Fe–O_{oxo} bridge. The weighted average values of these resonances, 13.0 and 4.9 ppm, agree very well with the corresponding lines observed in **5** and **6**. The difference between the Fe–N_{cis} and Fe–N_{trans} average bond lengths in $[Fe_2O(O_2CCH_3)_2(TMIP)_2]^{2+}$ is 0.03 Å, and in **5** it is 0.04 Å.[31a] Thus, the trans influence of the short Fe–O_{oxo} bond is similar in the structures of both **5** and $[Fe_2O(O_2CCH_3)_2(TMIP)_2]^{2+}$. These results suggest that the magnetic equivalence of the imidazole rings in **5** and in the TMICMe analogue **6** is not due to accidental degeneracies but rather to a fluxional process, perhaps solvent dependent, in which the rings cis and trans to the bridging oxo ligand are exchanging rapidly on the NMR time scale. This possibility was not further investigated.

Summary and Conclusions. The flexible dicarboxylate ligand $MPDP^{2-}$ forms complexes having a discrete $\{Fe_2O(MPDP)\}^{2+}$ core using $HB(pz)_3^-$, BIPhMe, or TMICMe as the terminal ligands. The structure of **3** indicates that the dicarboxylate ligand does not distort the core geometry, which is essentially identical with that of the acetate analogue $[Fe_2O(O_2CCH_3)_2\{HB(pz)_3\}_2]$, **1**. As a consequence, the spectroscopic and magnetic properties of the two complexes are nearly identical. Use of $MPDP^{2-}$ ligand in place of monocarboxylate anions with bidentate ligands, B, has facilitated access to $[Fe_2O(MPDP)B_2Cl_2]$ complexes under conditions that previously gave only tetranuclear species.[11] Importantly, the iron coordination environment in these dinuclear complexes approximates that of the iron center in Hr, which binds O_2 as hydroperoxide and exogenous ligands.[6] The general utility of the present synthetic method is demonstrated by the preparation of related complexes with both dipyridine and the more biomimetic polyimidazole ligands. Changes in terminal ligation, from NNN to NNCl and from N(pyridine) to N(imidazole), alter the characteristic properties of the $\{Fe_2O(MPDP)\}^{2+}$ core primarily because of structural and ligand field strength modifications.

Electrochemical studies of **3** indicate that, although the $MPDP^{2-}$ ligand may stabilize a reduced dinuclear species as well as an electrochemically reversible ferric complex, reductive decomposition occurs to form $[Fe\{HB(pz)_3\}_2]^+$. These observations reinforce the notion that strategies to mimic the functional chemistry of diiron oxo protein cores must prevent formation of mononuclear or other thermodynamically stable species. Remarkably different stability properties were observed for the dipyridine versus the polyimidazole $[Fe_2O(MPDP)B_2Cl_2]$ complexes. An additional desirable property of the polyimidazole complexes is their solubility in hydrogen-bonding solvents. Physical measurements in MeOH revealed that solvents capable of hydrogen bonding to the oxo bridge have little affect on the electronic and magnetic properties of the $\{Fe_2O(MPDP)\}^{2+}$ complexes.

Finally, the present study has afforded the first example of terminal ligand exchange for the $\{Fe_2O(O_2CR)_2\}^{2+}$ core in the reaction of $[Fe_2O(MPDP)(4,4'\text{-}Me_2bpy)_2Cl_2]$ with $KHB(pz)_3$. Chemistry at the terminal positions is known to be important in the biological activity of diiron–oxo proteins.[7c,d] The $[Fe_2O(MPDP)B_2Cl_2]$ compounds significantly augment the emerging class of biologically relevant $\{M_2O(O_2CR)_2\}^{2+}$ (M = Fe and Mn) compounds with labile terminal ligands in which such reactions can be investigated.[12,15,50]

(49) (a) Sahlin, M.; Gräslund, A.; Petersson, L.; Ehrenberg, A.; Sjöberg, B.-M. *Biochemistry* **1989**, *28*, 2618. (b) Sahlin, M.; Ehrenberg, A.; Gräslund, A.; Sjöberg, B.-M. *J. Biol. Chem.* **1986**, *261*, 2778.

Acknowledgment. This work was supported by U.S. Public Health Service Grant GM 32134 from the National Institute of General Medical Services. R.H.B. is grateful to the NIH for support under Training Grant CA-09112, and W.B.T. is grateful to the American Cancer Society for a postdoctoral fellowship. We thank Dr. G. C. Papaefthymiou for assistance in obtaining and analyzing Mössbauer data at the Francis Bitter National Magnet Laboratory, which was supported by the National Science Foundation. Resonance Raman experiments were carried out at the George R. Harrison Spectroscopy Laboratory at MIT, which is supported by grants from the NSF and the NIH.

(50) (a) Menage, S.; Girerd, J. J.; Gleizes, A. *J. Chem. Soc., Chem. Commun.* **1988**, 431. (b) Caneschi, A.; Ferraro, F.; Gatteschi, D.; Melandri, M. C.; Rey, P.; Sessoli, R. *Angew. Chem., Int. Ed. Engl.* **1989**, *28*, 1365.

Supplementary Material Available: Tables S1-S9, listing atomic positional and thermal parameters and complete bond angles and distances supplied for 3-5 (17 pages); Tables S10-S12, listing observed and calculated structure factor tables for 3-5 (93 pages). Ordering information is given on any current masthead page.

Contribution from the Department of Chemistry, University of Texas at Dallas, P.O. Box 830688, Richardson, Texas 75083-0688

Synthesis, Equilibrium, and Kinetic Properties of the Gadolinium(III) Complexes of Three Triazacyclodecanetriacetate Ligands

E. Brucher,† S. Cortes, F. Chavez, and A. D. Sherry*

Received May 18, 1990

Three new 10-membered-ring triaza tricarboxylate ligands have been synthesized and the formations of their Gd^{3+} complexes examined. The ligands 1,4,7-triazacyclodecane-*N*,*N*',*N*''-triacetate ($DETA^{3-}$), 9-methyl-1,4,7-triazacyclodecane-*N*,*N*',*N*''-triacetate ($MeDETA^{3-}$), and 9,9-dimethyl-1,4,7-triazacyclodecane-*N*,*N*',*N*''-triacetate (Me_2DETA^{3-}) have an unusually high first protonation constant (log $K_1 \approx 14$-15), and evidence is presented for the formation of a strongly hydrogen-bonded proton between the two nitrogens that share the propylene bridge in the monoprotonated forms of these chelates. Exchange of the hydrogen-bonded proton is slow below 0 °C, and its ^1H NMR signal has been detected. Complexation with Gd^{3+} is also slow, preventing determination of metal ion-ligand stabilities by potentiometry. Conditional stability constants for Gd(DETA), Gd(MeDETA), and Gd(Me_2DETA) were measured by using a proton relaxivity technique and compared with similar data for the 9-membered-ring macrocyclic complex Gd(NOTA). The rates of formation of Gd(DETA) and Gd(MeDETA) are similar, while Gd(Me_2DETA) forms more slowly. The rate-determining step of complexation is proton loss and rearrangement of a monoprotonated intermediate, formed in a fast preequilibrium reaction. Dissociation of the complexes takes place both in a spontaneous fashion and through a proton-assisted pathway. The rate of both processes decreases in the order Gd(Me_2DETA) ≫ Gd(NOTA) > Gd(DETA) > Gd(MeDETA). An increase in ring size from 9 to 10 and substitution of a methyl group onto a ring carbon of the ligand lead to increased kinetic stabilities of the complexes. The substitution of two methyl groups onto a ring carbon, however, results in a significant decrease in both the thermodynamic and kinetic stabilities of the resulting Gd^{3+} complex.

Introduction

The development of magnetic resonance imaging (MRI) and the successful use of the complex $Gd(DTPA)^{2-}$ for detecting tumors have resulted in a growing interest in the preparation and study of new Gd^{3+} complexes.[1] The properties of $Gd(DOTA)^-$ ($DOTA^{4-}$ = 1,4,7,10-tetrazacyclododecane-*N*,*N*',*N*'',*N*'''-tetraacetate), particularly its extremely low rate of dissociation, make this complex a very promising candidate for clinical use.[2] However, both $Gd(DTPA)^{2-}$ and $Gd(DOTA)^-$ are charged complexes and the osmolality of the solutions injected intravenously is quite high. In this respect, neutral complexes, formed with the cyclic triaza tricarboxylate ligands would be more favorable. The complex Gd(NOTA) ($NOTA^{3-}$ = 1,4,7-triazacyclononane-*N*,*N*',*N*''-triacetate) has a higher water proton relaxivity than $Gd(DTPA)^{2-}$ or $Gd(DOTA)^-$, but both the thermodynamic and kinetic stabilities of Gd(NOTA) are lower than those of the DTPA or DOTA complexes.[3-5] This is likely a consequence of the small size of the cyclononane ring of this chelate.[6]

We have now prepared several new triaza tricarboxylate ligands in an attempt to determine the effect of macrocycle size and rigidity on the complexation properties of these ligands.[7] We report here our data on three new 10-membered-ring chelates, 1,4,7-triazacyclodecane-*N*,*N*',*N*''-triacetate ($DETA^{3-}$), 9-methyl-1,4,7-triazacyclodecane-*N*,*N*',*N*''-triacetate ($MeDETA^{3-}$), and 9,9-dimethyl-1,4,7-triazacyclodecane-*N*,*N*',*N*''-triacetate (Me_2DETA^{3-}) (see I).

The basicity of one nitrogen in $DETA^{3-}$, $MeDETA^{3-}$, and Me_2DETA^{3-} was found to be unusually high. While this work was in progress, the preparation of $DETA^{3-}$ was published,[8] but neither its protonation constants nor its complexation properties were studied in detail.

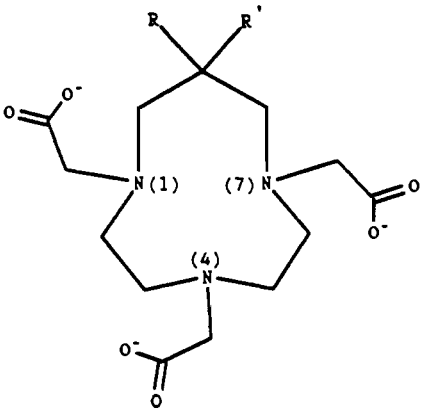

R = CH_3; R' = H — $MeDETA^{3-}$
R = CH_3; R' = CH_3 — Me_2DETA^{3-}

I

Experimental Section

Synthesis and Characterization of Ligands. 1,4,7-Triazacyclodecane-*N*,*N*',*N*''-triacetate (DETA) was prepared as previously described.[9] The

* To whom correspondence should be addressed.
† On leave from Lajos Kossuth University, Debrecan, Hungary.

(1) Lauffer, R. B. *Chem. Rev.* **1987**, *87*, 901.
(2) Desreux, J. F.; Barthalomy, F. F. *Nucl. Med. Biol.* **1988**, *15*, 9.
(3) Geraldes, C. F. G. C.; Sherry, A. D.; Brown, R. D., III; Koenig, S. H. *Magn. Reson. Med.* **1986**, *3*, 342.
(4) Cacheris, W. P.; Nickle, S. K.; Sherry, A. D. *Inorg. Chem.* **1987**, *26*, 958.
(5) Brucher, E.; Sherry, A. D. *Inorg. Chem.* **1990**, *29*, 1555.
(6) Hancock, R. D.; Martell, A. E. *Chem. Rev.* **1989**, *89*, 1875.
(7) Cortes, S.; Brucher, E.; Geraldes, C. F. G. C.; Sherry, A. D. *Inorg. Chem.* **1990**, *29*, 5.
(8) Craig, A. S.; Helms, J. M.; Fankowsky, K. F.; Parker, D.; Beeley, N. R. A.; Boyce, B. A.; Eaton, M. A. W.; Millican, A. T.; Millar, K.; Phipps, A.; Rhind, S. K.; Harrison, A.; Walker, C. *J. Chem. Soc., Chem. Commun.* **1989**, 794.

0020-1669/91/1330-2092$02.50/0